Vibration Frequency Measurement by DNA-shaped Metamaterial Array

By

Xinxiang Zong

A thesis submitted to
the Faculty of Graduate Studies
in partial fulfilment of
the requirements for the degree of
Master of Science

Department of Mechanical Engineering
Faculty of Graduate Studies
University of Manitoba
Winnipeg, Manitoba

May 2023

Abstract

Detecting the vibration frequency is a fundamental task of vibration testing. Constrained by the working principle relying on the electrical signal, the current vibration measurement techniques are either expensive, time-consuming, not portable, or susceptible to electromagnetic interference. This research proposes a novel vision-based vibration frequency measurement technique by introducing a mechanical metamaterial array. The array is consisting of a certain number of DNA-shaped metamaterials. Due to the flexible design of metamaterials, the design parameters of different DNA metamaterials can be adjusted to achieve their distinct vibration patterns under certain excitation frequencies, especially the different rotating angles. As a result, when the metamaterial array is attached to a vibrating object, the vibration frequency from the target can be estimated by comparing the vibration patterns of different individual metamaterials. The design of the DNA-shaped metamaterial is first optimized by finite element analysis (FEA) to achieve a significant rotation angle during vibration. Selective laser sintering (SLS) 3D printing is used to create finalized DNA-shaped metamaterials that are subsequently assembled into array structures. The persistence of vision technology is utilized to provide a clear view of the rotational motions. Frequency visualization is achieved through time-lapse photography experiments along with a new data processing algorism to resolve the frequency from rotating motions of the metamaterials array. The simulation and experiment results

demonstrate the feasibility and efficiency of the proposed methodology for rapid, non-contact, wireless detection of the vibration frequency of an object.

Acknowledgment

I would like to express my sincere gratitude to all the individuals and institutions who have contributed to the completion of my thesis titled "Vibration Frequency Measurement by DNA-shaped Metamaterial Array." This research project would not have been possible without the generous support, guidance, and encouragement of numerous individuals and institutions.

First and foremost, I would like to express my deepest appreciation and gratitude to my supervisor, Dr. Nan Wu, for his invaluable guidance, expertise, and unwavering support throughout the research project. His profound knowledge, valuable insights and constructive feedback have shaped the direction of my work and ensured its quality and impact. I am deeply grateful to him for his guidance and dedication to my academic growth.

I am grateful to the members of my thesis committee, Dr. Yunhua Luo and Dr. Xihui Liang, for their valuable time, insightful comments, and critical evaluations. Their expertise and academic contributions have enriched my research and made my investigation more comprehensive. Their guidance and feedback have been invaluable in refining my ideas and improving the overall quality of this thesis.

I would like to acknowledge the financial support provided by the University of Manitoba and Natural Sciences and Engineering Research Council of Canada, which enabled me to conduct the experiments and obtain the necessary resources. I am grateful to the faculty, staff and research facilities of the Price Faculty of Engineering. Their commitment to academic excellence and provision of a conducive research environment is invaluable throughout the research process.

I express my heartfelt gratitude to my families and friends for their unwavering love, encouragement and understanding. Their support and trust in my abilities have given me the motivation to overcome challenges and gain inspiration in this research process.

Finally, I express my appreciation and gratitude to everyone involved in making this research a reality. Your contributions are critical and have left a lasting impact on my academic and personal growth.

Contents

List of Tables

List of Figures

List of Symbols and Abbreviations

Symbols

t	Top plate thickness
w	Top plate width
d	Diameter of beam
L	Length of beam
ρs	Density of top plate
ρd	Density of beam
d/L	Thickness to length ratio
α	Angle alpha
θ	Angle theta
Wn3	Third natural frequency
Uz	Maximum Vertical vibration amplitude
Rz	Maximum rotation angle
E	Stiffness/Young’s modulus

Abbreviations

NC	Number of unit cell
X	The average angle of rotation
Hz	Hertz

LDV	Laser Doppler vibrometer
MM	Metamaterial
AM	Additive manufacturing
VMS	Vibration mode shapes
FV	Frequency visualization
FE	Finite element
FEM	Finite element modal
FEA	Finite element analysis
SLS	Selective laser sintering
DAQ	Data Acquisition

Chapter 1

Background Introduction and Literature Review

Machines are widely used in today's industry and need to be monitored in real-time or periodically maintained to eliminate potential safety hazards and prevent damage from unexpected breakdowns. Structural health monitoring can detect existing or potential machine failures and prevent them, such as unbalance, wear, misalignment, cracks, and defects in machine components. In the aspect of health monitoring and diagnostic methods, the commonly used methods in recent years include oil analysis, vibration signal analysis, particle analysis, corrosion monitoring, thermal imaging analysis, acoustic signal analysis, and wear debris analysis. Among these approaches, vibration analysis is considered as the commonly used method and more than 82% of the fault diagnosis techniques are based on vibration analysis (Kumar et al., 2018; Henriquez et al., 2014; Immovilli et al., 2010; Zhang et al., 2012). With vibration signal analysis, the machine being inspected does not need to be stopped or disassembled. By obtaining the vibration signal of the target and analyzing it in comparison with a reference signal, it is possible to detect the existence of a machine fault. Generally, the existing vibration analysis health monitoring process can be divided into three main steps, which are data acquisition, signal processing, and fault recognition (Mohd Ghazali & Rahiman, 2021). In the data acquisition phase, different vibration collectors are used to acquiring time domain signals of various mechanical parameters of the target under vibration, such as velocity, acceleration, and displacement, through their various operating principles. In the data processing phase, these signals are converted into frequency domain data by Fourier transform and other methods to obtain the final vibration data of the object.

1.1 Vibration Frequency Acquisition

The common vibration acquisition methods can be divided into two groups, contact and non-contact methods as shown in Figure 1, depending on the type of installation of the sensor on the object to be measured (Ferrer et al., 2013). The contact method needs to install the sensors on the component, which often has inevitable errors due to the masses of the sensors. As an alternative, the non-contact method has better performance in different measuring environments since it does not need the installations of sensors in the structure. But the cost of the non-contact method is usually expensive (Henriquez et al., 2014). Based on the research findings, it has been determined that existing frequency measurement methods possess certain limitations, particularly when applied in the field of rapid frequency measurements. Therefore, the primary objective of this study is to conduct a comprehensive literature review of traditional and novel frequency measurement techniques, highlighting their respective advantages and disadvantages. Subsequently, this study identifies the current shortcomings of these methods and proposes new methods to effectively address these limitations.

Figure 1

Tree Diagram of the Vibration Measurement Device

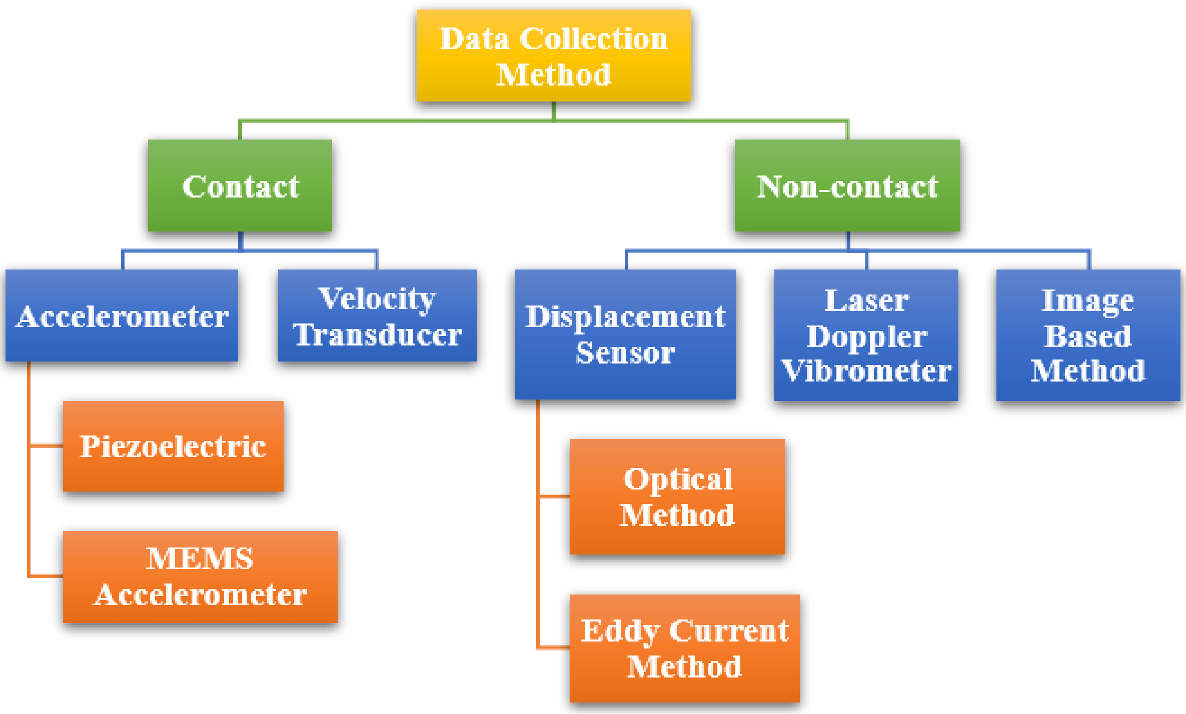

1.2 Contact Method

Accelerometers are usually preferred as a contact method due to their simplicity, high reliability, sensitivity, and low price. These devices transmit the local acceleration signal at the specific point where they are attached to the piezoelectric material or electrodes located inside the accelerometer to produce an electrical signal proportional to the acceleration (Cheung et al., 2014). Similar to accelerometers, velocity transducers measure the relative velocity of the object by measuring the voltage generated by the coil and magnet (Goyal & Pabla, 2015). An internally suspended magnet generates a magnetic field and when speed is fed to the sensor, a coil moving in the field will induce an electromagnetic field in the coil, thus generating a voltage proportional to velocity. Since they are contact devices, they can be difficult to use in situations where space is at a premium, and the measurement results on small-weight and weak target objects can be compromised. In addition, depending on their working methodology, they cannot be used in environments with strong electromagnetic interference (García et al., 2010).

1.3 Non-contact Method

Alternatively, displacement sensors are used as non-contact devices. It collects vibration data by measuring the relative distance between the target object and the sensor by detecting the displacement of the element that is emitted and reflected. Depending on the elements used, there are two types of sensors that are commonly used, called optic displacement sensors and linear proximity sensors, where the elements are light and magnetic flux, respectively (Mohd Ghazali & Rahiman, 2021). Although they have high sensitivity, wide dynamic range, and high reliability. But they are usually expensive, and their further signal processing steps require complex and expensive equipment. The distance between the sensor and the object is limited, and the signal may be interfered by environmental influences (Goyal & Pabla, 2015). To reduce the environmental influence and increase the measurement distance, a low-cost fiber optic displacement sensor for industrial applications was developed by Saimon et al. (2019). A more precise approach called Laser Doppler vibrometer (LDV) works on the principle of the laser Doppler concept (Saimon et al., 2019). If the light is scattered from a moving object, its frequency is changed slightly. LDV emits and receives the reflected laser beam. The frequency and phase differences between the backscattered beam and the reference beam are analyzed and provide the velocity and displacement of the test object vibration. Although LDV provides the best displacement and velocity resolution and can be used for long-distance measurements without compromising signal quality, the application of LDV in machine monitoring and diagnostics is limited by its expensive price and poor portability (Mohd Ghazali & Rahiman, 2021). In the 21st century, image-based methods are becoming a reliable alternative to non-contact vibration measurements. The principle of its operation is to use the intensity of light to measure the displacement of an object. When an object is vibrating, the intensity of the light at its edges changes as the object moves. By recording and tracking the movement of the measuring point, the vibration displacement curve of that point can be obtained (Hild & Roux, 2006). Although the method can directly derive the time domain vibration spectrum of the target, the critical aspect is the requirement for high-resolution cameras that may not always be available or cost-effective. Moreover, this approach requires a large amount of image data, resulting in extensive computations and extended data processing time during the data processing phase. Due to the limitations of the experiment equipment, this method can only measure the vibration of an object in the two-dimensional plane (Son et al., 2021; Son et al., 2015).

1.4 Current Shortcomings

Overall, from the literature, conventional vibration frequency detection methods measure vibration frequency by detecting the time domain signal of the vibration and converting it to frequency domain signal by either Fourier series analysis, Windowing function or Wavelet transform. All approaches require complex calculation processes to obtain the vibration frequencies. Furthermore, during the data acquisition phase, all sensors in contact methods are electronic components that have to be connected by wires and fixed to the target, which often has inevitable errors due to the masses of the sensors. This limits the size of the target that can be measured. The non-contact methods usually require specialized equipment and are often expensive. Therefore, it is necessary to investigate a novel vibration frequency detection approach. This method requires a significantly simpler data processing phase, a relatively low cost of equipment, a more intuitive method of data acquisition and a relatively smaller and more portable equipment size. Based on the findings of recent research, it has been demonstrated that certain novel technologies, including DNA-shaped structures and metamaterial (MM) array, show promise in addressing the current limitations.

1.5 Metamaterial

The concept of MM was first introduced by Victor Veselago in 1967 (Slyusar, 2009, p. Ukraine), and since then the field has undergone significant expansion and evolution. While the properties of conventional materials depend on their chemical composition and internal structure, the properties of MMs depend on their macroscopic structure, not on the material they are made of. MMs possess properties not found in nature, such as negative Poisson's ratio or negative refractive index. Combinations of repetitive cell patterns with precise shapes, geometries, dimensions, orientations and arrangements confer extremely high controllability of the material's properties. MMs have been developed rapidly in recent years due to their excellent performance and are widely used in photonic devices, microwave sensors, antennas, and energy harvesting (Suresh Kumar et al., 2021). Due to the exotic electromagnetic properties of MMs, their use as electromagnetic sensors has attracted the research interest of academics in recent years (Chen et al., 2012). The study by Huang et al. indicates that incorporating MMs into microwave sensor design can result in improvements in both sensitivity and resolution (Huang & Yang, 2011). Furthermore, with the development of additive manufacturing (AM), MMs have been closely associated with AM in recent years, which enables rapid manufacturing and experimentation of MM prototypes, especially in the fabrication of complex MMs structures (Fan et al., 2021).

1.6 Objectives

Combining the characteristics of the above technique, this research proposes a new fast vibration frequency measurement method based on pure mechanical responses, including a mechanical structure for data acquisition and a novel data processing logic. Through the combination and application of technologies such as vibration mode shapes (VMSs), AM, DNA-shaped structures, and MMs, a MM structure consisting of a certain number of different DNA-shaped rotating columns in an array under vibration is developed. The new approach can be considered as an image-based contact method but with simpler data acquisition and processing phases compared to traditional electronic sensors called frequency visualization (FV). Rather than a time-frequency conversion process, this method quantifies the magnitude of the frequency by the mechanical behavior of the array structure of the MM composition.

1.7 Basic Principle

Each object has its own resonant frequency and VMS. By observing the vibration shape of the target object and comparing it with its VMS, the vibration frequency of the object can be roughly estimated. The problem is that the VMSs of a complex structure are difficult to analyze, and the vibration frequency can be estimated only if the vibration shape of the whole structure can be observed. Furthermore, it is almost impossible to observe objects with very small vibration amplitudes and compare them with their VMS. Therefore, attaching a structure with a known VMS to the target is a feasible method. These two objects will have the same vibration frequency. Without knowing the vibration shape of the entire structure, the vibration frequency of the target can be estimated simply by observing the vibration shape of the attached structure. The method proposed in this research is to attach a MM array structure consisting of a certain number of DNA-shaped columns to the vibrating object. This structure contains multiple styles of columns which can rotate under vibration, and each type of column is designed to have a different resonant frequency. The vibration frequencies of the target object are determined by comparing and analyzing the different vibration patterns among the rotating columns, which is also referred to as FV in this thesis.

As the first study to use MMs for frequency visualization, the application of the above techniques allows the new frequency measurement technology to inherit their advantages. Compared to traditional methods, the new DNA structures significantly reduced the weight of the attached device (Liu et al., 2018). The high controllability characteristic of MMs makes the vibration shape and resonance frequency of the unit MM becomes easily adjustable (Suresh Kumar et al., 2021). This means that the structure can theoretically be adapted to measure any frequency domain. In addition, the use of AM enables the dimensions and weight of the MM array to be controlled (Fan et al., 2021). Therefore, with the guarantee of printing quality, the whole structure can be made very small and light, which can be used to measure the vibration frequency of light or weak objects. This fabrication method also enables high fabrication efficiency and rapid experimental validation of the samples. The most important point is that the only electronic device used in this method is a cell phone with time-lapse capability, which significantly reduces the cost of measurement.

This research first determines the exact specification of the proposed DNA-shaped MMs through simulation, then the final structure is fabricated, and the associated algorithm is used to estimate the frequency, followed by experiments to verify the feasibility of the method. Finally, a simulation study is carried out to discuss the detection range of the experimentally validated Finite element (FE) model.

Chapter 2

Rotating DNA Like Structure for Vibration Monitoring

2.1 Design Scope

Due to the absence of current research on the use of MM technology for rapid vibration frequency detection, combined with the inadequacy of conventional vibration frequency detection methods. The objective of this research is to develop a new technique for the detection of vibration frequencies of objects using MMs and AM technology, including the fabrication of a new data acquisition device and the development of an algorithm for the data processing phase. The desired objective for the prototype is to be able to rapidly detect vibration frequencies in the 50-100hz range with an error of less than 10%.

The initial structure is based on Yang's research and is designed as shown in Figure 2 (Yang, 2019). Firstly, some structural improvements have been made to make it feasible for vibration testing, then simulations are carried out to optimize the performance of the unit structure under vibration and to obtain the modified structure, which is then printed by AM and further refined according to the printing quality, then the single structure is formed into MM array and tested for vibration and then further optimized according to its performance. After the finalized MM array is fabricated, the vibration test is conducted to verify the accuracy of the technology.

Figure 2

Design and Improvement Flow Chart

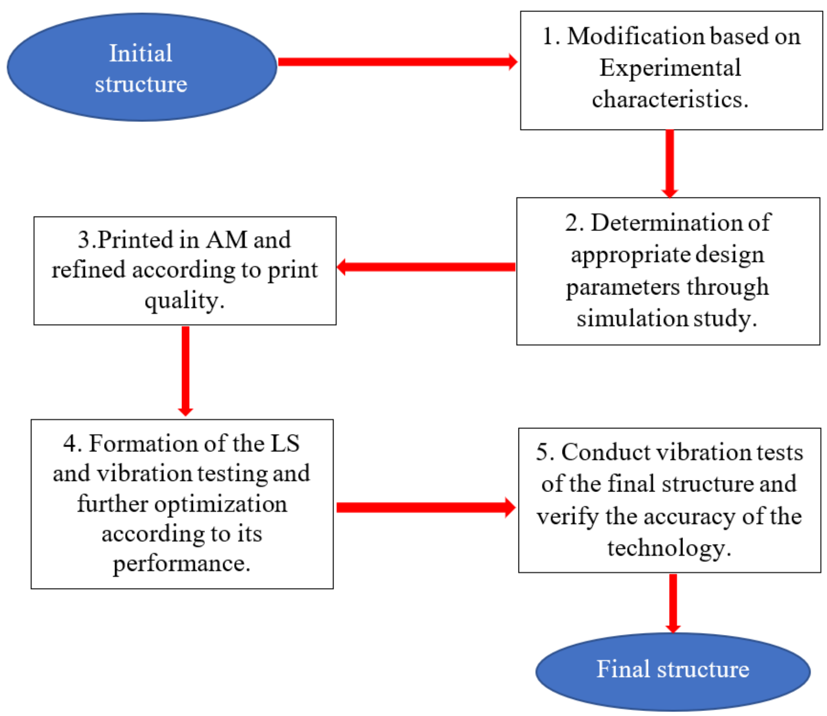

2.2 Rotating Column Design and Modal Analysis

By combining the shape of DNA with an origami mechanism, yang has recently developed a DNA-like chiral structure that theoretically achieves an infinite twist per axial strain (Yang, 2019). The structure consists of several identical unit cells and has excellent tensile-torsional coupling properties and resistance to global buckling. Therefore, based on the characteristics of this structure, it is expected that the DNA-like chiral structure will exhibit a special vibrational torsional feature in one of its vibrational modes.

The proposed twisted structure is constructed based on the DNA-like chiral structure (Yang, 2019), with two end plates at the top and bottom. The benchmark for the construction was to give it a better dynamic performance, making it more suitable for vibration testing. Specifically, as illustrated in Figure 3, the structure starts with a basic unit cell constructed from beam elements which can be considered as approximately half of an octahedron, except the face of the octahedron are consisted of eight identical equilateral triangles while the unit cell of the structure is composed of four identical equilateral right-angled triangles. The key parameters of the unit cell are angle alpha (α), angle theta (θ), length (L), and diameter (d), which controls the angle of the equilateral right triangle, the angle between two horizontal beams of the unit cell, the length of the right-angled side of the right-angled triangle and the beam diameter, respectively. Next, as shown in Figure 3(b), the second unit cell in orange is stacked on top of the first unit cell. These two cells share an edge highlighted in blue and its two endpoints, and an intersection point locates at the center of its top and bottom edge beams. Similarly, continuing to pile up N units, we can obtain a DNA-like chiral structure as shown in Figure 3(c). By removing half cells of the unit cell at the top and bottom of the chiral structure and placing two plates at each end, the original structure for the simulation study can be obtained. The key consideration regarding the structure is that the midpoints of the top and bottom plates need to coincide with the central axis of the DNA structure in order to avoid buckling and asymmetric torsion.

In order to identify the vibrational characteristics possessed by a DNA-like chiral structure, a modal analysis of the original structure was carried out. The first four VMSs of the structure are shown in Figure 4. In the case of the first two vibration modes of the structure, the vibration behavior is approximately the same except for the different directions of oscillation of the top plate. However, in the third mode shape, the top plate not only moves up and down, but also rotates at the same time. This is a significant difference from the other vibration patterns, and this vibration characteristic makes the third VMS easier to observe and differentiate from the other VMSs. In addition, since the other mode shapes are basically about the oscillation of the DNA structure and there is no vibration in the vertical direction, the vibration shape that the structure mainly exhibits in the case of vertical excitation at the bottom will be the third mode. Based on this finding, the vibration mode of the structure at the third resonant frequency can be used as the reference vibration pattern of the structure. The current vibration frequency of the structure can be estimated by comparing the rotation angle of the top plate with the reference pattern. Further, it is possible to vary the design parameters of individual structures so that each structure has a different third resonant frequency, and by arranging multiple individual structures together and applying a bottom excitation to them, the excitation frequency can be more conveniently and accurately estimated by comparing the vibration patterns between the different individual structures and by comparing their own reference patterns. When measuring a vibrating object, the bottom of the structure is attached to the top surface of the object; the vibration is along the longitudinal direction of the DNA structure and transferred from the structure to the DNA MM. The measured vibration frequencies are also corresponding to the up and down vibration perpendicular to the top surface of the target structure.

Figure 3

How the Unit Cells are Organized into the Final Structure

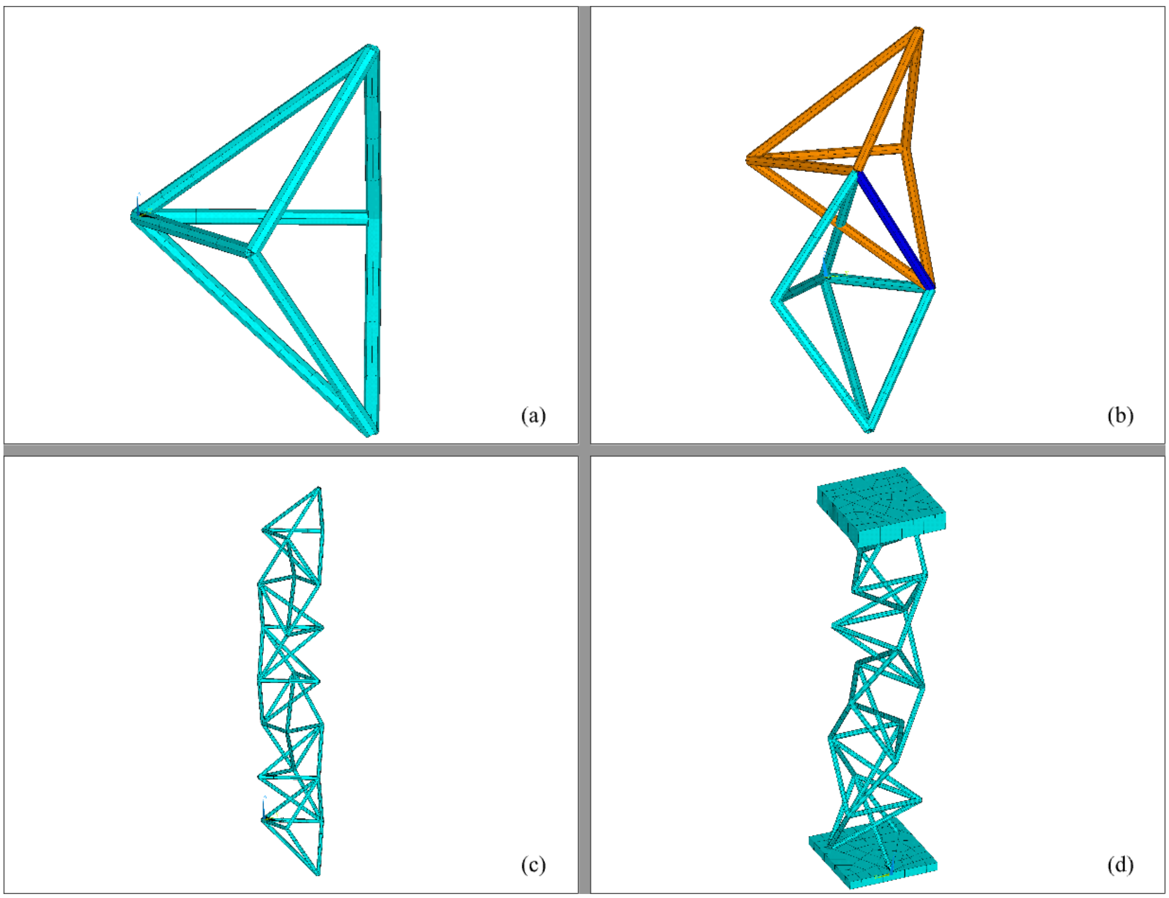

Note. One cell of the DNA structure, how the second cell is stacked on top of the previous one, a DNA structure consisting of seven cells and a sample of the rough structure are shown in figure(a), (b), (c) and (d) respectively.

Figure 4

The First, Second, Third and Fourth Mode Shape of the DNA Structure are Shown in Figure(a), (b), (c) and (d), Respectively

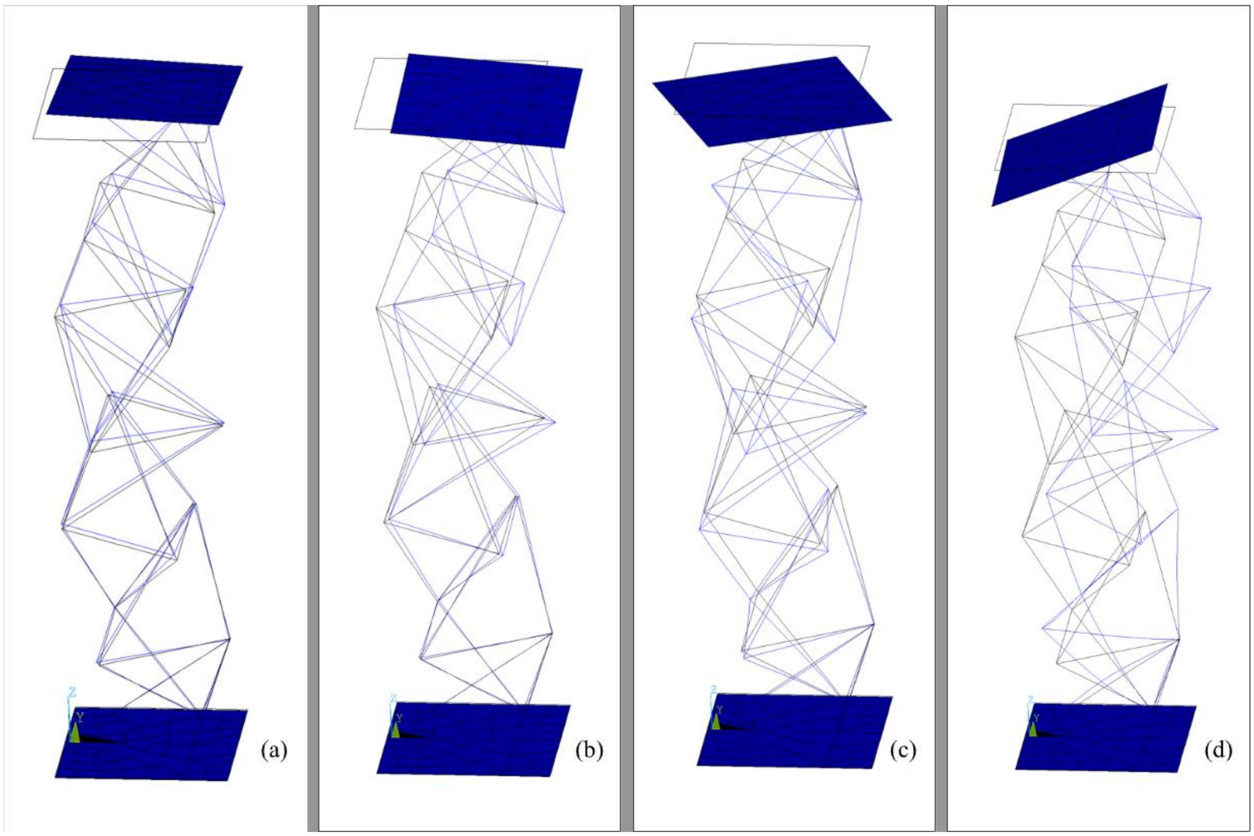

Chapter 3

DNA Column Design Tuning for Obvious Rotating Through FEA

After establishing the working principle of the structure, the design needs to be improved to establish the structure suitable for further experiments. The content of this section describes the process of improving the structure through a simulation study, referred to as the third step in Figure 2. The basic philosophy of the process is to modify and finalize the design parameters of individual structures through simulation in order to achieve specific objectives. The objectives included achieving a maximum vibration torsion angle while keeping the vertical amplitude of the top plate constant, making the structure as small as possible but easy to manipulate by hand for further experimental stages.

3.1 Design Parameters to be Tuned

The design parameters for a single structure can be summarized in two parts, with a total of twelve parameters as shown in Figure 5(b). Although the material properties of the base plate also have an effect on the vibration pattern of the structure. However, as the bottom plate is fixed to the test bench and is designed to be very thin, the effect of the bottom plate on the structure is negligible and therefore the design parameters of the bottom plate are not taken into account. The remaining twelve design parameters can also be combined and reduced depending on the effect on the structure. The thickness (t) and width (w) control the dimensions of the top plate and the density (ρs) controls the weight of the top shell. As the top plate is considered to be a weight block that adds to the structure, the only important design parameter is the weight of the top plate. Therefore, the three design parameters are summarized into one variable, which is the thickness (t) while the other parameters are set as constants. For the design parameters of the DNA structure, both the diameter (d) and length of the beam (L) are considered to control the thickness-to-length ratio (d/L) of the beam, therefore they can be reduced to one parameter, which is length (L). Due to the limitations of printing technology, the density (ρb) and stiffness (E) of the DNA structure are difficult to control, so these two design parameters are set as constants and are not considered during parameter study. As shown in Figure 5(a), the angle alpha (α) and angle theta (θ) control the angle of the equilateral right triangle, the angle between two horizontal beams of the unit cell, respectively. In summary, the above twelve design parameters reduce to five by the analysis, which are top shell thickness (t), beam length (L), angle alpha (α), angle theta (θ) and number of unit cells. The next step is to conduct simulations for each of these five parameters. The first step in the simulation study is to set the reference design parameters which will be used in each simulation. During the simulation for the specified parameters, the only variable is the specified parameter itself, while the other parameters remain constant to the reference parameters. By altering specific parameters, the relationship between the parameter changes and the vibration performance can be simulated. This includes the effect of parameter changes on the third resonant frequency (Wn3), The maximum displacement of the top plate in the vertical direction at the third resonant frequency of the structure (Uz), and the angle of rotation of the top plate in response to the third resonant frequency excitation (Rz).

The structure is made up of two types of elements, the DNA structure consists of beam elements and the top and bottom plates are considered as shell elements. All material models applied are isotropic and linear. The simulation methods are modal and harmonic analysis respectively, where modal analysis is used to obtain the third natural frequency of the structure for different design parameters and harmonic analysis is used to calculate the maximum vibration response amplitude of the structure having different design parameters near the third resonant response situation using frequency sweeps. In the modal analysis, the base plate is set to be completely fixed, while in the harmonic analysis, the base plate can be moved in the vertical direction. The reference design parameters are shown in Figure 5(b). Since the material properties for AM are unknown, the damping ratio and stiffness are obtained from the literature.

Figure 5

Design Parameters for the Single Structure

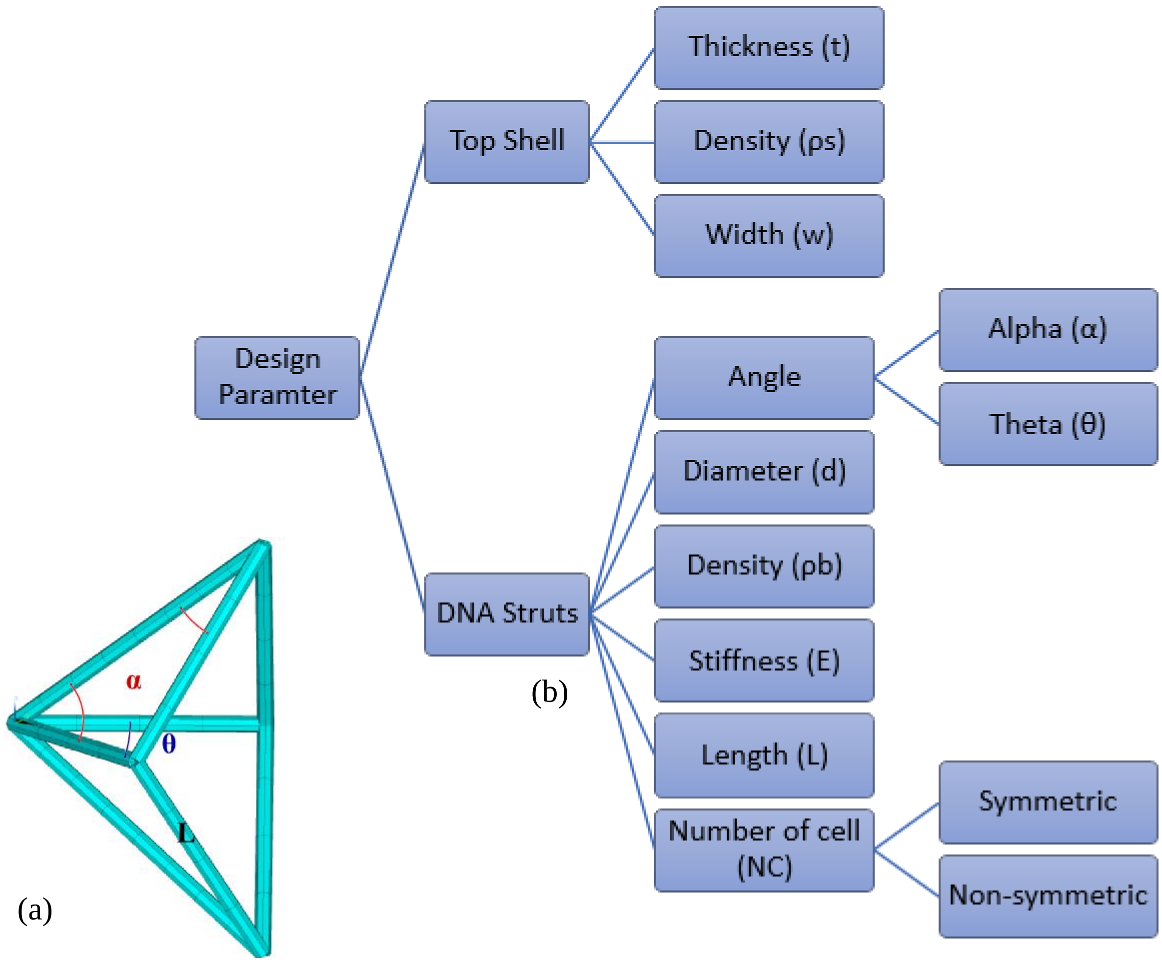

Table 1

Reference (Default) Design Parameters of a Single Rotating Column

No	Design Parameters	Value
1	Structure Height	44.09082 mm
2	w	10.9119 mm
3	d	0.36 mm
4	α	45 deg
5	θ	60 deg
6	L	9 mm
7	t	3 mm
8	Bottom plate thickness	0.3 mm
9	Frequency independent material damping ratio	0.07
10	Stiffness	145 MPa
11	NC	7

3.2 Simulation Results for Design Optimization

Before proceeding with the simulation study, a convergence study is required to confirm the appropriate element sizes for the finite element model (FEM). Figure 6 shows the maximum rotation angle of the top plate at the third resonance for a specific single structure at different mesh sizes. The thickness of the top plate is 5 mm and a vertical amplitude excitation of 10% of the structure height is applied to the bottom plate. Since the length of the beams that comprise the DNA structure are not identical. The definition of elemental size is presented by the divisions on the beams. The simulation results show that the maximum von Mises stress does not vary much and converges when the number of segments is greater than 4. Furthermore, to avoid excessive computational time, all lines were divided into 5 segments. Therefore, the minimum mesh length for the FEA is 1.2728mm and the maximum mesh length is 1.8mm.

Figure 6

Convergence Study of maximum rotation angle of the top plate at third resonance with Different Mesh Sizes

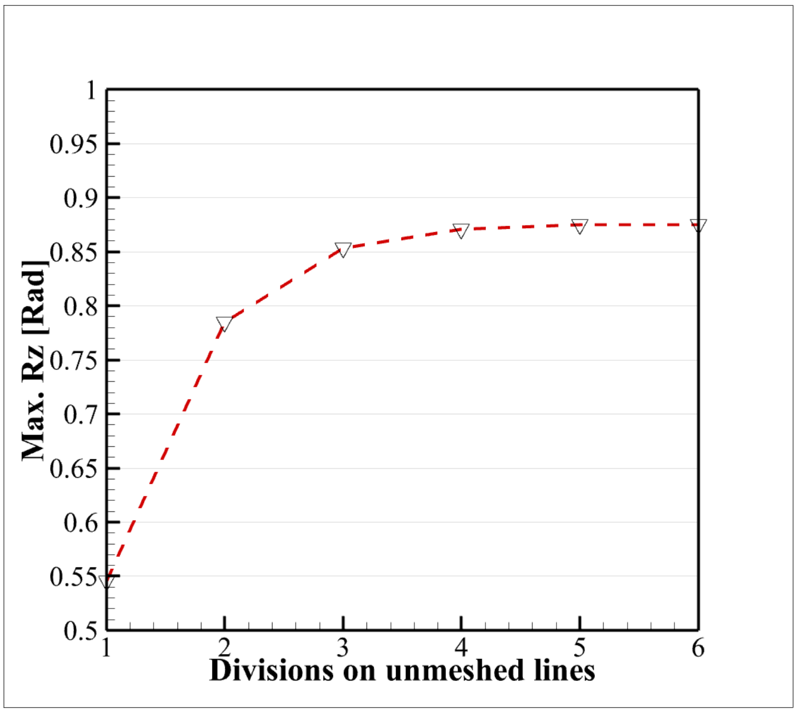

Figure 7 shows the third natural frequency of the structure in relation to the first four design parameters. All four design parameters have the opposite effects on the third natural frequency. Figure 8 shows the effect of variations of thickness, length, angle α and angle θ on the vibration response amplitude (linear motion) of the top of the structure in the vertical direction while 10% base motion excitation is applied at its third resonant frequency. The results are obtained from the Frequency sweep test, with 10% vertical base motion excitation with sweep frequencies ranging from 20hz to 200hz, in sub-steps of 0.1hz for every magnitude of design parameters shown in Figure 5. The maximum displacement values for each sweep result are then extracted and the displacement versus design parameter curves are plotted. From Figure 8, it can be seen that changes in T and L have a fairly weak effect on Uz. Changes in α have the opposite effect, while θ has a positive effect on Uz. As shown in Figure 9, for Rz with the same simulation study as Uz, both T and L have opposite effects, while α and θ have a functional effect.

NC refers to the number of cells that make up the DNA structure and can be classified into two approaches, symmetrical and non-symmetrical, depending on the way in which the structure is built. For the case of non-symmetrical, the only variable is NC. In contrast, for the case of symmetry, the DNA structure needs to be vertically symmetrical from its midpoint, which means that the unit cells locate at the top and bottom of the structure, which means that the angle between the bottom cell unit and the top cell unit needs to be 0 or 360 degrees. From the stacking mechanism of the unit cells, it follows that angle θ is the parameter that controls the angle between adjacent cells. Therefore, the magnitude of θ needs to vary with the number of cells to ensure symmetry of the structure, i.e. 360/(NC-1). In addition, α needs to be greater than θ/2, so that α is fixed at 45 when NC is greater than 5 but becomes 47.5 when NC is less than or equal to 5. In summary, the variables in the study process for the symmetric case are NC and θ. The simulations show that in the symmetric case, NC has a functional effect on Wn3 and Rz and an opposite effect on Uz. Whereas for the asymmetric case, NC has an opposite effect on Wn3, almost no effect on Uz, and a positive effect on Rz.

Figure 7

Effect of Variations of Thickness, Length, Angle α and Angle θ on the Third Resonance Frequency of the Structure are Shown in Figures (a),(b),(c) and (d), Respectively

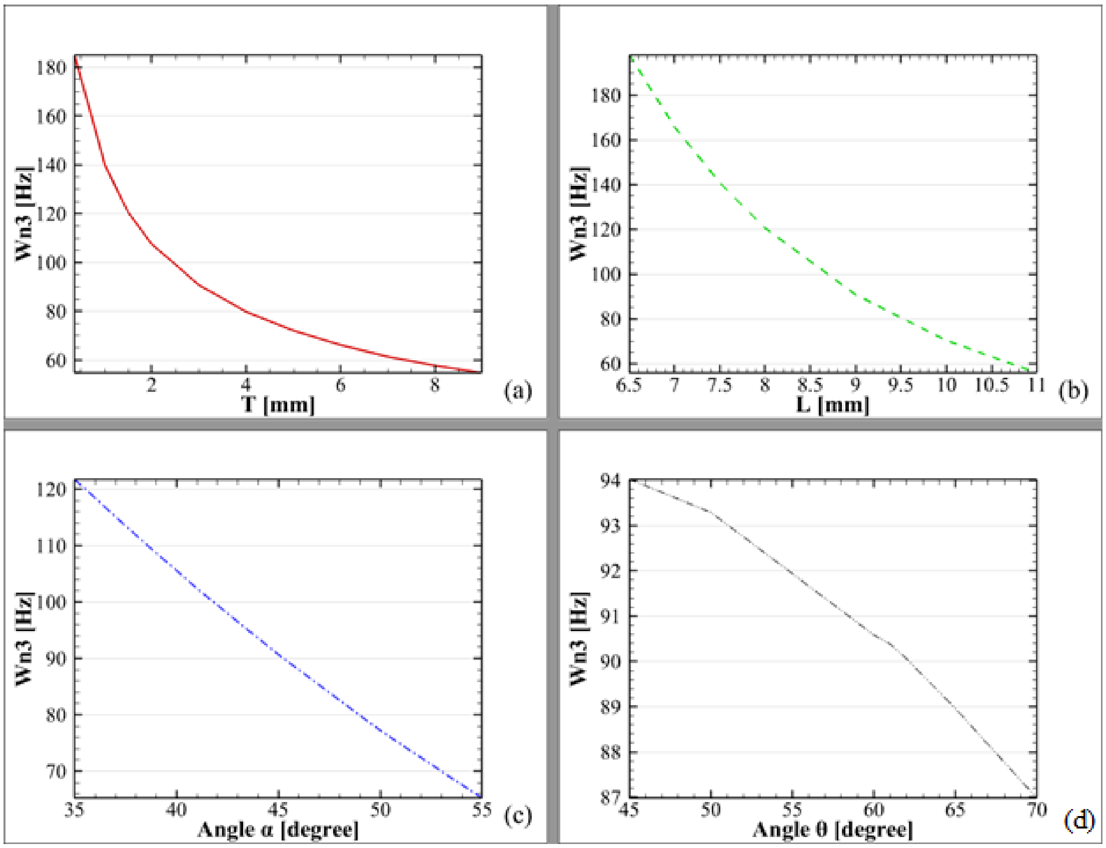

Note. Except for the variables in the x-coordinate, the design parameters in Figure 5 are consistent with the reference dimension in each simulation case.

Figure 8

Effect of Variations of Thickness, Length, Angle α and Angle θ on the Vibration Amplitude (Linear Motion) of the Top of the Structure in the Vertical Direction at the Third Resonant Frequency are Shown in Figures (a),(b),(c) and (d), Respectively

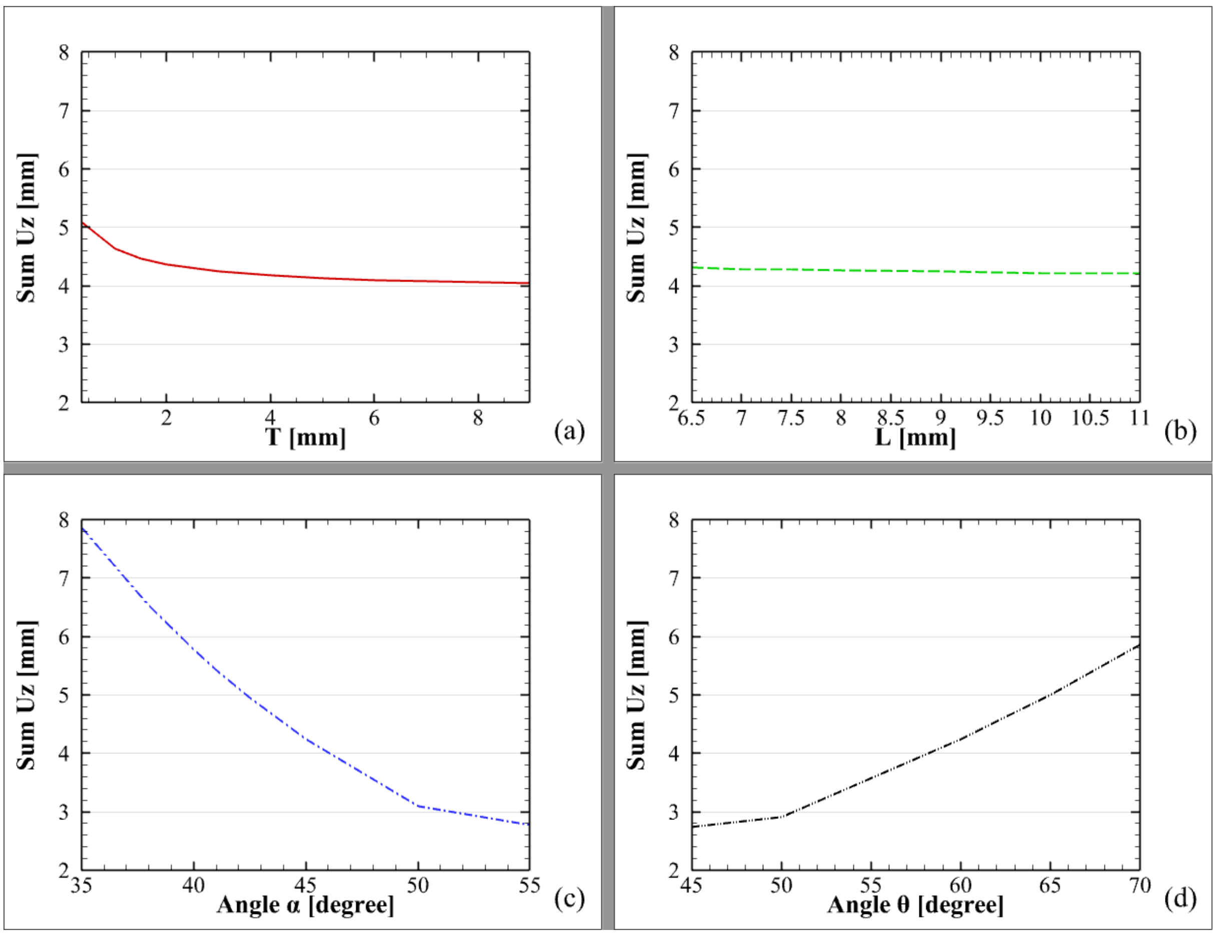

Note. The design parameters in Figure 5 are consistent with the reference dimension in each simulation case, except for the variables in the x-coordinate.

Figure 9

Effect of Variations of Thickness, Length, Angle α and Angle θ on the Vibration Angle Amplitude of the Top of the Structure in the Horizontal Direction at the Third Resonant Frequency are Shown in Figures (a),(b),(c) and (d), Respectively

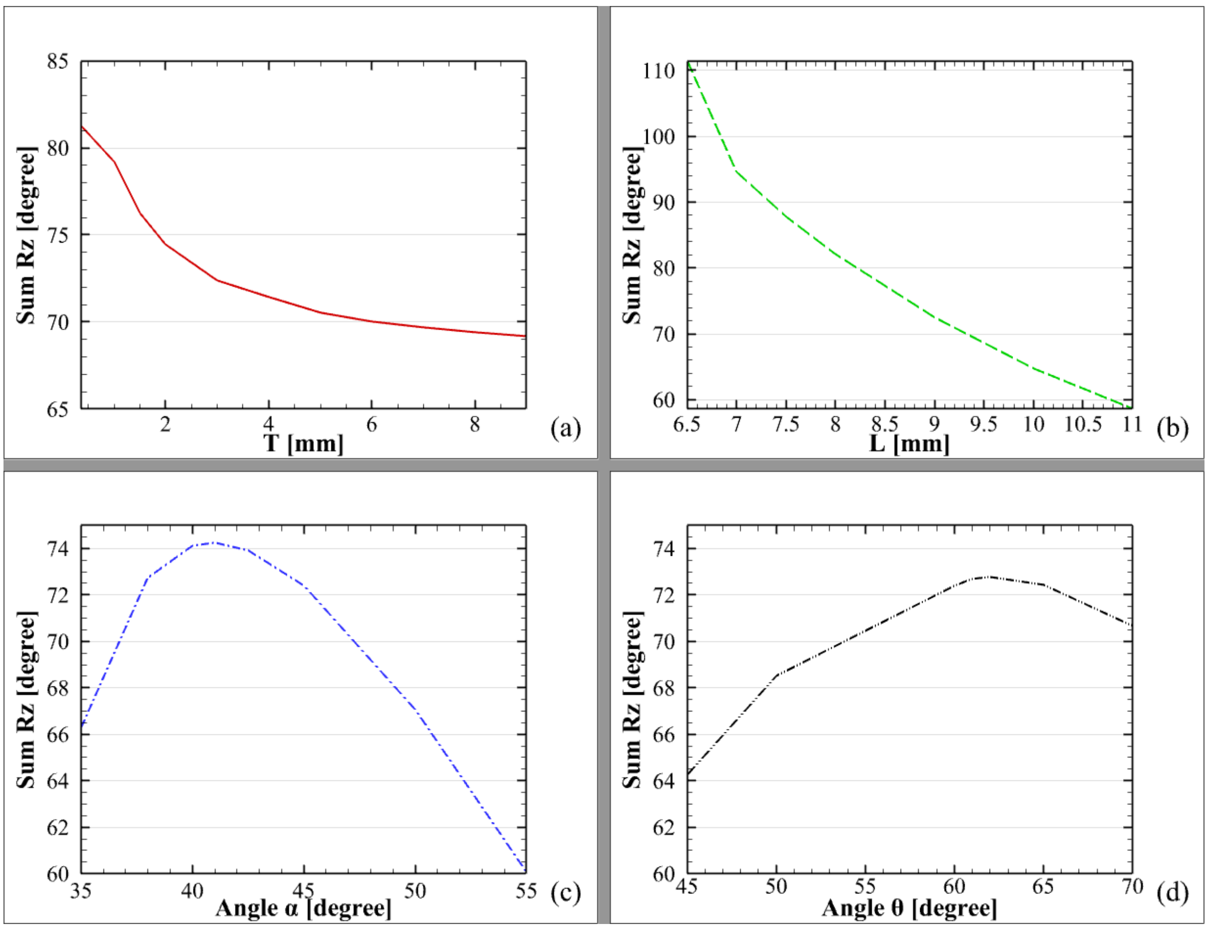

Note. The design parameters in Figure 5 are consistent with the reference dimension in each simulation case, except for the variables in the x-coordinate.

Figure 10

Effect of Variation in the Number of Structural Spirals on the Third Resonance Frequency, Top Plate Vertical Amplitude and Horizontal Angle Amplitude of the Structure are Shown in Figures (a),(b) and (c), Respectively

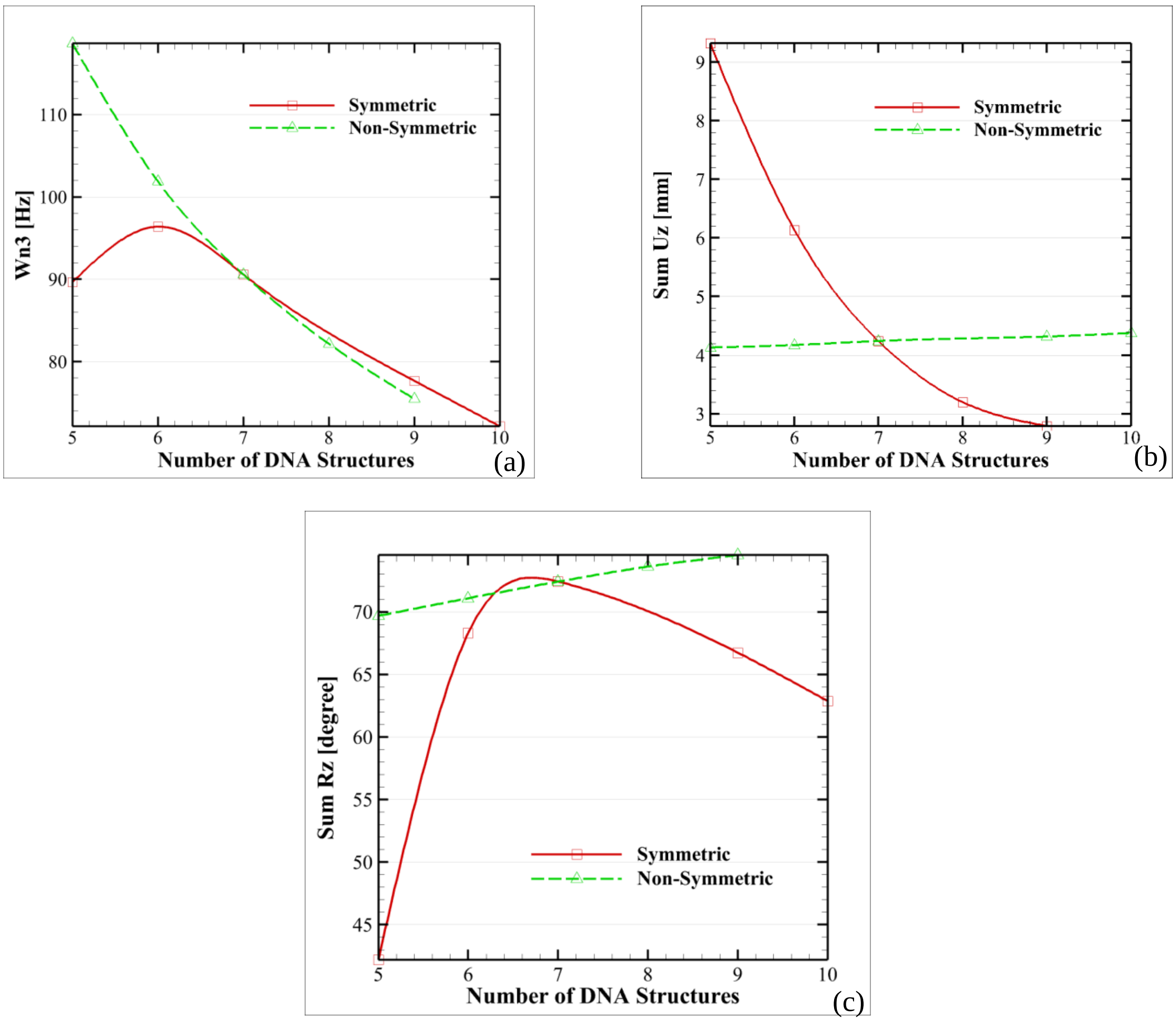

Note. For the symmetric case, the variables are NC and angle θ. For the Non-symmetric case, the only variable is NC. While the other design parameters in Figure 5 are consistent with the reference dimension in each simulation case.

The relation between design parameters and structural vibration performance are shown in Table 2. According to the improvement criteria mentioned at the beginning of this chapter, the thickness of the top plate is specified as the only variable and the other parameters will be assigned to a suitable value based on the results of the simulation and will remain constant throughout the subsequent experiments, in order to keep the shape of the single structure approximately the same for easy alignment and observation. The final structure is approximately 44 mm high and consists of 7 unit cells, the value of L is set to 9 mm, d is set to 0.36 mm, α is set to 45 degrees, and θ is set to 60 degrees. The FEM for the finalized design for the experiment process is shown in Figure 11. The actual properties of the material from which the structure is fabricated will be examined and discussed in the next section.

Table 2

Influence of Design Parameters on Structural Vibration Characteristics

Design parameter	**Structure height**	**Third natural frequency**	**Max vertical amplitude Uz**	**Max rotation angle Rotz**
T	No/quite weak effect	Opposite effect	Opposite effect	Opposite effect
L	Positive effect	Opposite effect	Opposite effect	Opposite effect
Angle α	Positive effect	Opposite effect	Opposite effect	Functional effect
Angle θ	Opposite effect	Opposite effect	Positive effect	Functional effect
NC sym	Positive effect	Functional effect	Opposite effect	Functional effect
NC Non-sym	Positive effect	Opposite effect	No/quite weak effect	Positive effect

Figure 11

FEM for the Finalized Design by Simulation

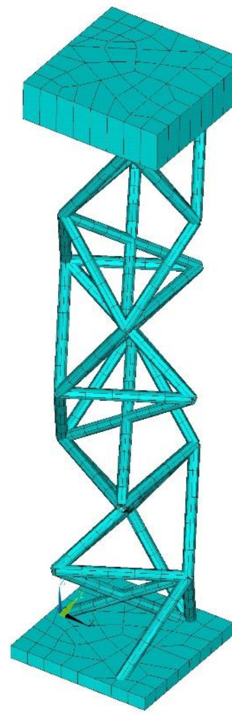

Chapter 4

Prototyping the Testing Samples by 3D Printing

This section includes the AM process of the single DNA-like strut structure, the further modification based on print quality and vibration behavior, the experimental determination of the material properties used for AM, and DNA-like strut top plate design based on the persistence of vision. Then, the final MM array composed of multiple DNA-like struts for conducting physical vibration frequency measurement is identified and described.

4.1 Single DNA Structure Modification for Prototyping and Testing

The equipment used for AM is the Noble 1.0A laser printer from XYZPRINTING, where single structures are printed vertically, and the printed structures are suspended upside down on the printing platform. The initial AM plan is to print the single structure from the bottom plate and then print it in its entirety, but due to the characteristics of the structure, the structure would rotate slightly when printed to the top plate, as the cross-shaped top plate applied a tensile load to the DNA structure. This would result in extremely poor print quality of the top plate. Therefore, the decision is made to print the structure in two parts, which are then assembled together. Depending on the price of the resin and printing consumption, the cost of producing a single DNA column structure can range from C$0.1 to C$0.3. The printing and modification processes are illustrated in Figure 12. As shown in (a) and (b), the top plate and the rest of the single structure are printed separately. The printing quality for the DNA structure is low due to the d of the beam of the finalized FEM design being too low. Through multiple printing tests, it has been found that the quality of the beams can only be guaranteed when they have a minimum diameter of 1mm. As a result, the diameter of the beam increases to 1mm as illustrated in (c). This variation increases the d/L of the beam and, according to the results of the simulation study, increasing the d/L increases Rz, which is consistent with the direction of improvement. This type of structure was then manufactured in proportions of 1.5x, 1x, 0.8x, and 0.5x to determine which is suitable for operation, with the 1.5x scale structure being determined as the final structure.

Figure 12

Finalization Process of 3D Printed Structure

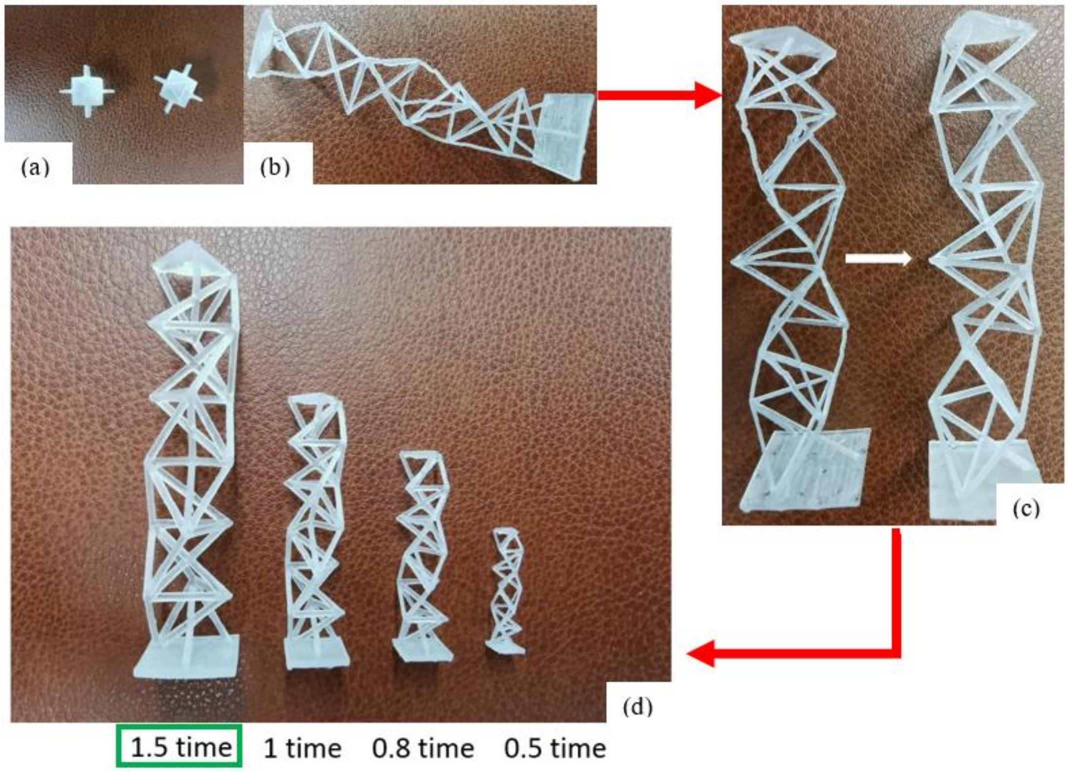

Note. 3D printed samples of the first part and second part of the preliminary design structure are shown in figure(a) and (b). Due to low print quality, the ratio of beam length to diameter increases, as shown in figure(c). The structure in figure(c) with a scale of 1.5x is selected as the final structure as shown in figure(d).

4.2 Determination of Material Properties

The material used for AM is the clear standard resin from XYZPRINTING. As the properties of the material are not shown on the official website, some experiments are required to determine these properties. The Young's modulus and density of the material are determined experimentally, while the Poisson's ratio and damping ratio are obtained from the literature, due to the limitations of the experimental equipment.

4.2.1 Young's Modulus and Validation

Young's modulus determines the stiffness of the structure and has an effect on the natural frequency and vibration amplitude of the structure. The tensile test is applied to determine the Young's modulus of the structure.

The usual specimens used for tensile testing are dumbbell-shaped specimens. Depending on the type of material used for manufacture, the standard specification for this experimental specimen is obtained from ISO 37:2017, which is for rubber, vulcanized or thermoplastic materials. Depending on the dimensions of the SLS printer, the dimensions of the dumbbell-shaped specimen are determined as type 2, as shown in Figure 13. The results in Figure 14 show that the Young's modulus of the cured resin is 66.72MPa.

Figure 13

Dimensions for the Test Specimens in Millimeters

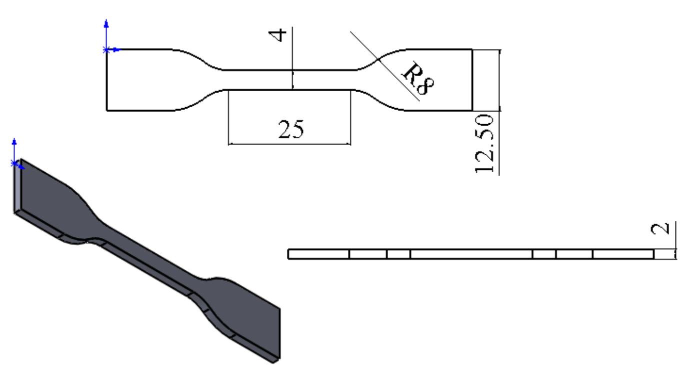

Figure 14

Stress-Strain Curve by First Tensile Test

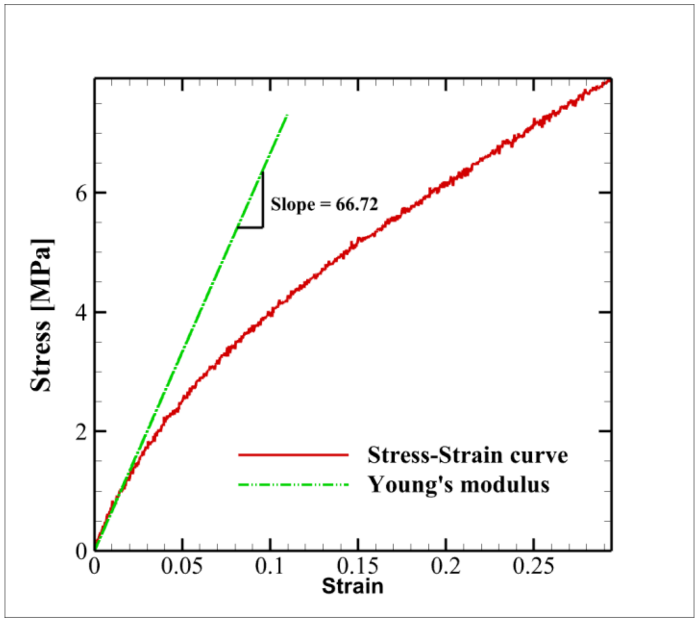

To verify the Young's modulus obtained from tensile tests, an experimental modal analysis is conducted, and the natural frequency results are compared with the ones from FEA. The experiment setup is shown in Figure 15. The purpose of this experiment is to roughly measure the third natural frequency of a single rotating column. The measured frequency is then compared with the simulated third natural frequency, which is obtained by applying the young modulus derived from the experiment. If the third natural for both experiment and simulation do not differ much from each other, the experimental result is considered reasonable.

The single rotating column is fixed on the shaker through a thick metal bar and a base motion excitation in the vertical direction is applied with frequencies ranging from small to large, from 30Hz to 200Hz at 1Hz per sub-step. A metal tape is stuck on the top of the column as shown in Figure 15(b) for the purpose of reflecting the laser signal emitted from LDV placed above the structure as shown in Figure 15(a). The LDV detects the vertical velocity of the top plate of the structure and converts the signal to the Simcenter system via the 6-channel LMS DAQ in Figure 15(c), which finally displays a time-domain signal about the velocity. By extracting the average amplitude of the velocity corresponding to each frequency, a frequency domain curve about the velocity can be obtained.

According to the operating principle of the shaker, the amplitude of vibration decreases with increasing frequency at a constant shaker input voltage. Furthermore, based on previous harmonic analysis, the vertical amplitude of the top plate increases and reaches a maximum at resonance as the excitation frequency approaches the third natural frequency, and decreases as the excitation frequency moves away from the third natural frequency. Therefore, it can be expected that the magnitude of the velocity decreases as the frequency increases and slows down as the excitation frequency approaches the third natural frequency. After the frequency has just exceeded the third natural frequency, there will be a significant increase in the slope of the frequency domain curve. The experimentally obtained curve shown in Figure 16 verifies the theory, where the third natural frequency is expected to be 96 Hz, while the simulated third natural frequency with Young's modulus of 66.72 MPa is only 33 Hz, which differs dramatically from the experimental results. Therefore, it is considered that the current tensile test is not suitable for measuring the Young's modulus of this structure. After research, a special specimen more appropriate for use in this tensile test is designed and fabricated.

Figure 15

Experimental Setup for Modal Analysis

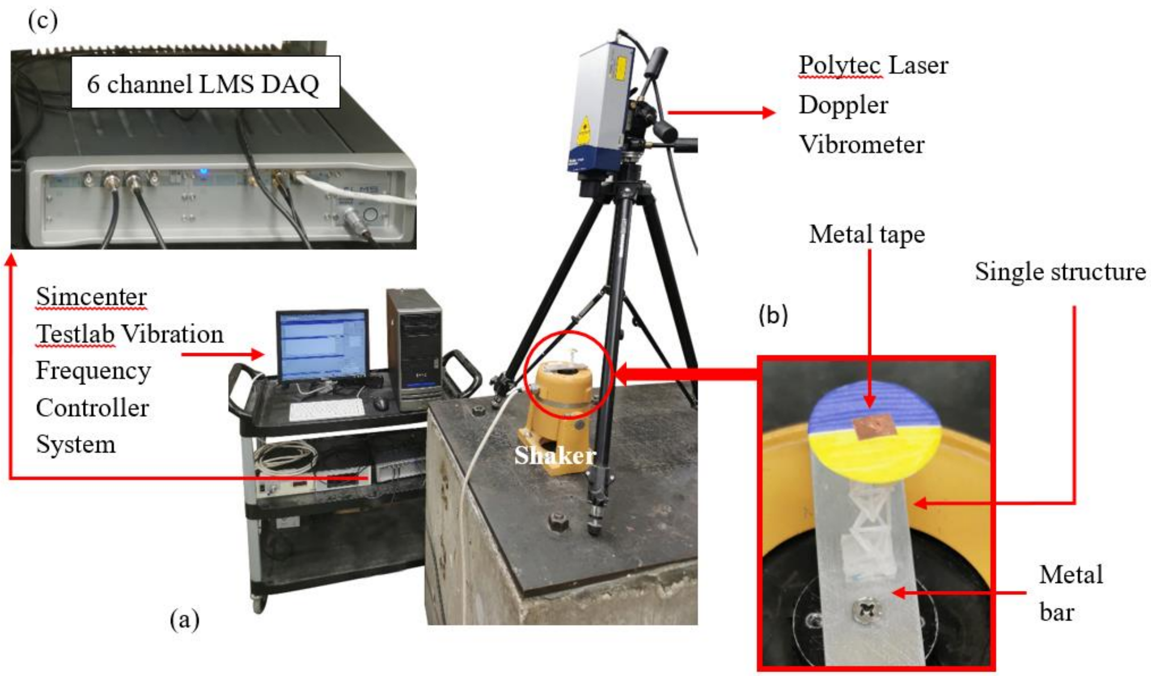

Note. (a) Experimental setup for modal analysis, (b) the single structure with a metal tape at the top for measuring vibration response, and (c) the 6-channel DAQ for data collection from vibrometer and outputting vibration signals from the controller system.

Figure 16

Vibration Amplitude Velocity for the Top Plate vs. Base Motion Excitation Frequency

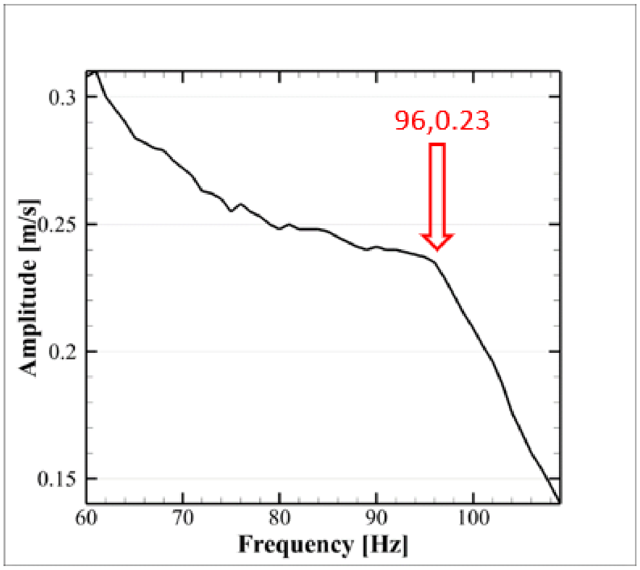

In order to match the printing direction of the structure, the test specimens are printed in the vertical direction. In addition, because of the small length and cross-sectional area of the structure's beam, traditional dumbbell-shaped test specimens are not suitable for measuring the structure's Young's modulus. By learning from the tensile sample used by Cao et al. (2018) in measuring the material properties of 3D printed lattice structures, the sample used in this tensile experiment is shown in Figure 17(a). The length used for the test section is 20 mm, and the diameter is 1.5 mm. The specimens are fixed in the MTS Insight Electromechanical-30 kN standard length machine and subjected to tensile testing. The resulting stress-strain curve for material demonstrates the characteristics of flexible materials and is illustrated in Figure 18. The measured Young's modulus of the 3D printed MM from the experimental modal analysis is estimated to be 550 MPa, which is more reasonable.

Figure 17

Dimensions for the Test Specimens in Millimeters are Shown in (A), Tensile Test Equipment is Shown in (B) and Fabricated Specimens are Shown in (C)

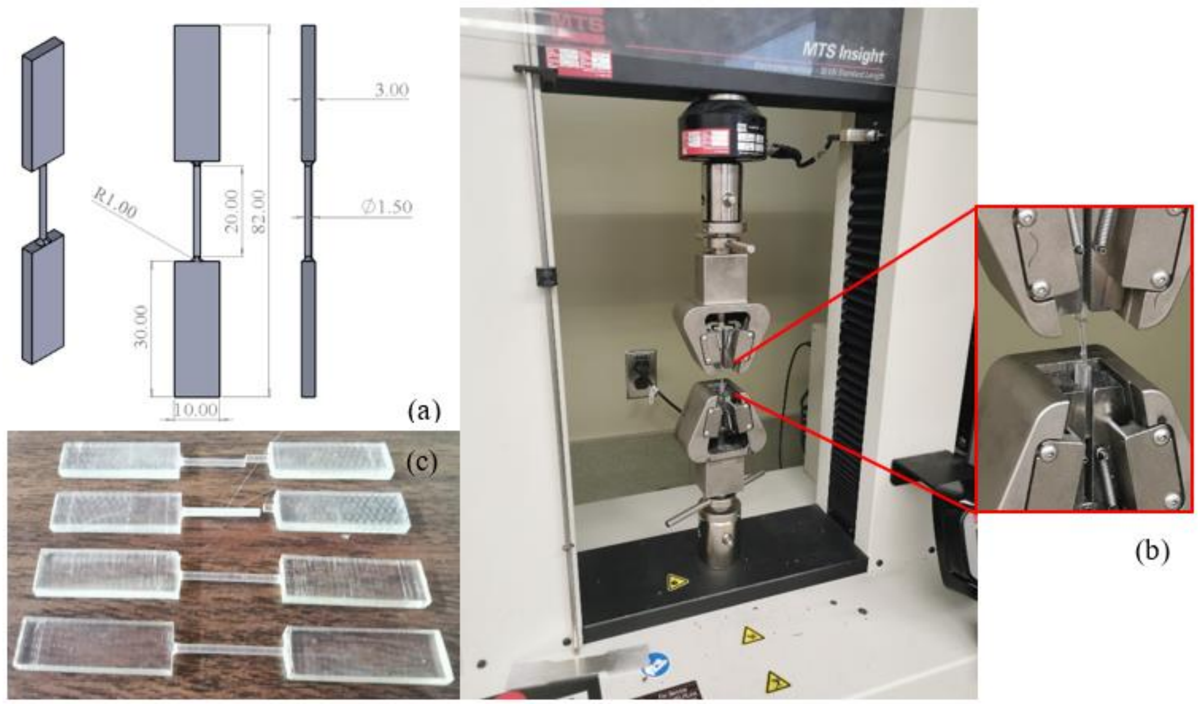

Figure 18

Stress-Strain Curve by Final Tensile Test

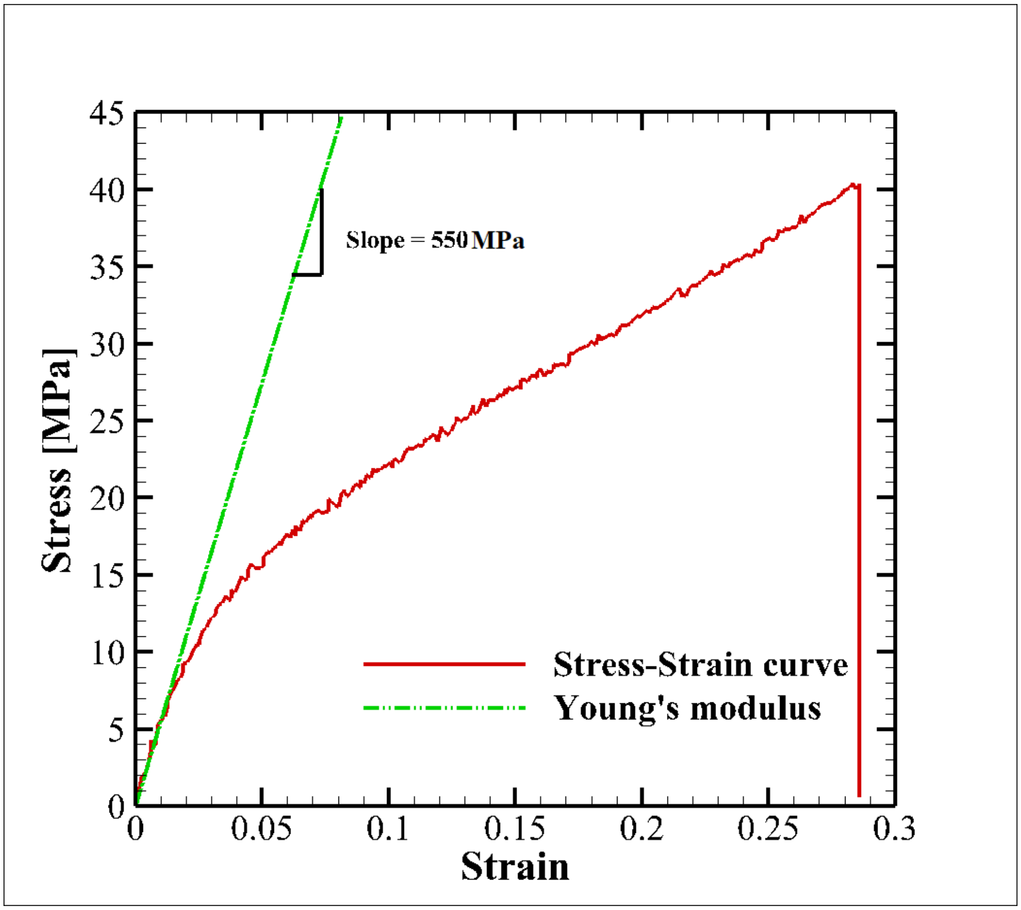

4.2.2 Density

The density of the material refers to the density of the printed material after it has fully cured and dried. Density mainly controls the mass of the top plate and is determined by the volume and mass of the structure. The reference structure is the top plate. The volume of the top plate is derived from the 3D file used to print the top plate. The mass of the printed top plate is measured by a digital mini scale which can measure down to milligrams. The density of the cured material is 1.36 mg/mm^3.

4.2.3 Poisson's Ratio and Damping Ratio

According to the resin manufacturer's specifications, the Poisson's ratio of a fully cured resin is between 0.33-0.35 (Saseendran et al., 2017), and the average is taken for this research, which is 0.34.

The damping ratio has no effect on the natural frequency of the structure, but mainly on the amplitude of the vibration. The magnitude of the damping ratio is derived from the study of Damping Properties of Flexible Epoxy Resin by Wang et al. (2008). Based on their research, the damping ratio is different for various temperatures and applied frequencies. Depending on the experimental environment of the material and the frequency range of the application, which is approximately 26 degrees Celsius and 50 to 100 Hz, the damping ratio decided to be applied in this study is 0.12.

4.3 Top Plates Design and Metamaterial Array Finalization

After the finalized single structure has been determined, a MM array containing multiple DNA structures as shown in Figure 19(a) is fabricated to test the performance of vibration. The main structure consists of three types of single structures with different top weights. These single structures were fixed to a test plate and a base motion excitation of 30 to 110 Hz is applied to them. It has been found that the rotation of the top plate on each of the single structures can be observed during the vibration of the structure, but it is difficult to distinguish and compare the magnitude of the rotation angle between the structures, thus making it difficult to measure the vibration frequency. One possible solution is to implement the quantization of vibration frequencies by measuring the angle of rotation or the vertical vibration amplitude for the top plate. In order to achieve this, the top plate of the structure needs to be improved. The original idea is to increase the area of the top plate so that the rotation of the top plate is more visible, but this does not enable quantization of the frequency and increases the size of the structure. In subsequent research, it is found that a possible application of the phenomenon of persistence of vision makes the angle of rotation quantifiable. The persistence of vision was discovered by the Belgian physicist Joseph Prato in 1835. One explanation for the persistence of vision is caused by the response times of the optic nerve. When there are short, high-frequency regular interruptions in the light emitted by an observed object, the visual system is unable to discern the differences between moments, and light and dark impressions merge together into a continuous impression of a scene with intermediate brightness. Its specific application is the shooting and projection of films (Buchan, 2013). The detailed implementation for the structure is to attach a circular piece of white paper to the top plate and place the center of the circular piece as close as possible to the center of the top plate, then divide this white paper equally into two semicircles along any center line and paint them in different colors. Theoretically, when the top plate is rotated forward and backward under vibration, the two colors will be mixed together and form a new color due to visual transient phenomena, thus showing an angle between the two original colors. This angle can then be considered as the rotation angle of the top plate, and by measuring this angle, the rotation angle of the top plate can also be quantified. Experiments are then conducted to test the feasibility of this theory, and different color combinations are tested to determine the color combinations provide clearer angles, including black and white, black and yellow, red and blue, purple and yellow, and a single black line on a white disc. The final results indicate that the angle of rotation is relatively clear when the two colors are complementary colors and the final color is decided as a combination of blue and yellow as shown in Figure 19(b) and (c). In the case of vibrations, the rotation of the top plate causes a light-colored area to appear between the yellow and blue areas. The angle can be clearly observed, and using the same principle, time-lapse photography can easily record the image of that rotation angle.

After obtaining the finalized structures, five types of single structures are manufactured, with two of each. The DNA structure is the same for all monolithic structures and the top plate specifications for each structure are listed in Table 3 and all structures are adhered to the test plate in the manner of Figure 20. The numbers marked on the structure represent the thickness of the top plate. Identical structures are arranged as non-adjacent as possible to prevent the effect of the vibration shape of the test plate on the structure. For each type of structure, due to the limitations of the printing technology, there are small differences in the weight of the top plate and the dimensions of the structure for the identical structures. Therefore, to eliminate any possible errors resulting from such differences, the weight of the top plate is measured and averaged prior to being adhered to the DNA structure, and subsequent experimental measurement results for the same structure are also averaged. The structure is then tested for vibration and the detailed experimental setup and methodology are expressed in the next section.

Figure 19

Top Plate Modification Process

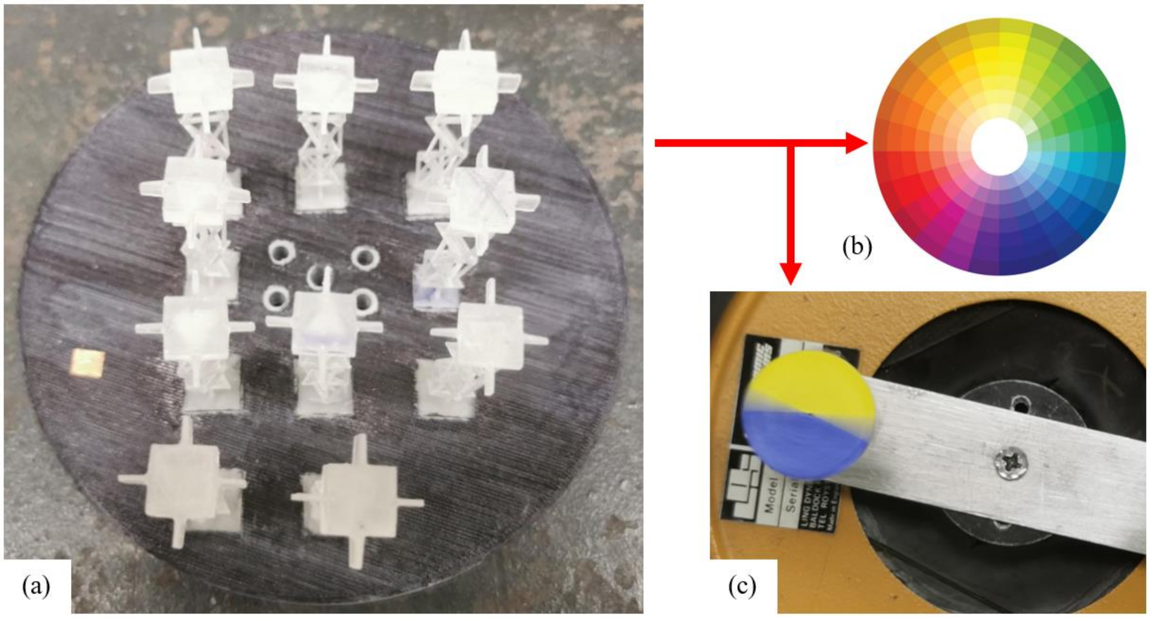

Note. The primary MM array with three different top plate thickness is shown in figure(a). The modified top plate utilizing persistence of vision and 180°complementary colors are shown in figure(b) (Color Circle Images – Browse 3,929,927 Stock Photos, Vectors, and Video, n.d.) and (c).

Table 3

Thickness of the top plate and its weight

Thickness	Mass 1 [g]	Mass 2 [g]	Average mass [mg]
1	0.385	0.379	382
2	1.144	1.132	1138
3	1.472	1.469	1470.5
4	1.858	1.878	1868
5	2.463	2.461	2462

Figure 20

Metamaterial Array Consisted by 5 Different Top Thickness, 1mm to 5mm

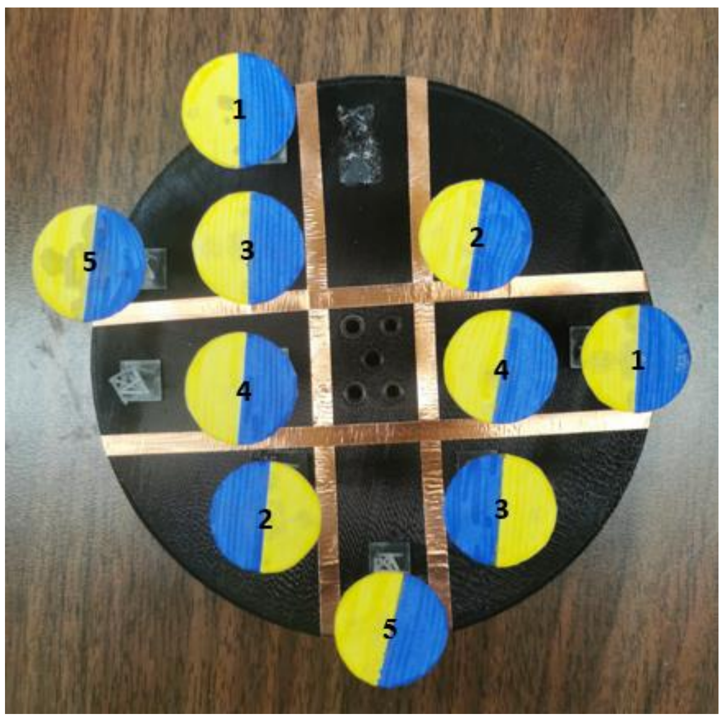

In order to validate the predictive capability and accuracy of the structure of the MM array in predicting the frequency of vibration, this section will implement vibration frequency measurements of the host structure of the array structure through vibration experiments. The intended process of the experiment is to apply a base motion excitation (simulating the vibration of the host structure attached by the MM array) with frequencies ranging from 50 Hz to 100 Hz, with 5 Hz for each sub-step, and to record the rotation angle of all the top plates by time-lapse photography. The recorded images need to be clear enough for image processing.

Chapter 5

Experimental Data Acquisition and Data Processing Methods for Frequency Measurement

5.1 Experiment Setup

All the devices and setup for the experiment are illustrated in Figure 21. The equipment used in this experiment includes a Simcenter Testlab Vibration Frequency Controller System, a 6-channel LMS DAQ, a sample structure fixed on a 3D printed test plate, and a smartphone with time-lapse photography. a shaker and a mobile phone holder. The vibration frequency controller system is used to output a signal to control the vibration frequency and send it to the LMS DAQ, where it is converted to reach the shaker and produce the specified vibration frequency. The shaker is tightly fixed to the table to avoid any effects due to self-oscillation. The test plate is bolted to the shaker. The recording device is a cell phone with a 400-megapixel time-lapse camera at 1080p (60fps), which is held directly above the top of the structure 40cm away from it by a holder to record vibration patterns. For each vibration frequency, the recording device performed a time-lapse of up to 30 seconds, and a photograph was obtained.

Figure 21

(a) Experimental Setup for Frequency Visualization Through Time-Lapse Photography and (b) The 6-Channel DAQ for Outputting Vibration Signals from the Controller System

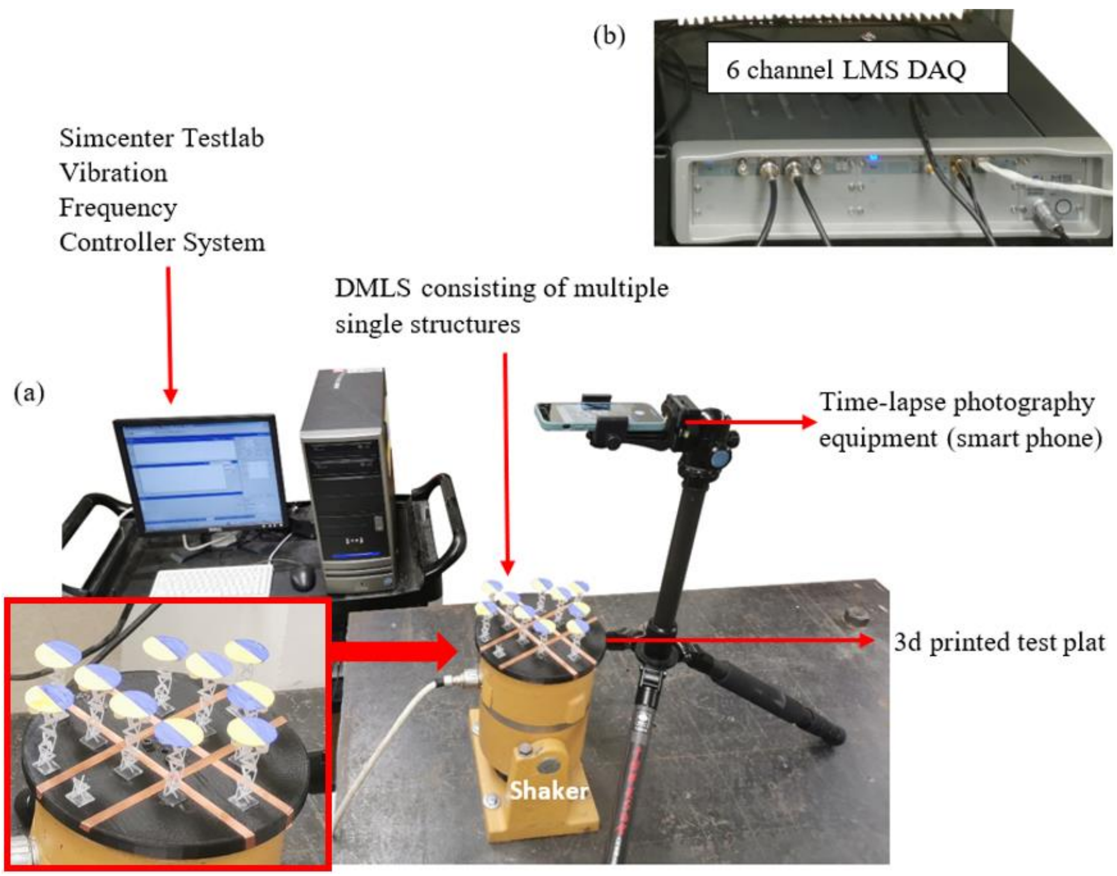

5.2 Data Processing for Frequency Visualization Through Time-lapse Photography

5.2.1 Image Processing

Once the photographs are obtained, these images are then imported into SolidWorks and the angles between yellow and blue areas are plotted and measured by tracing the lighter areas. Figure 22 shows a sample of image processing. During the process, three types of single structures with relatively large angles are chosen for angle measurement. Structures with 2mm, 3mm, and 4mm top plate thickness are chosen and the average rotation angles are 10.5025°. 8.9225°, and 6.55°. The obtained data is then imported to MATLAB code for frequency measurement.

Figure 22

Time Lapse Photo of the Top Structure with Bottom Excitation of 65HZ and Rotation Angles of Structures with 2, 3 and 4mm Thickness Blocks are Shown in Figure(a) and (b)

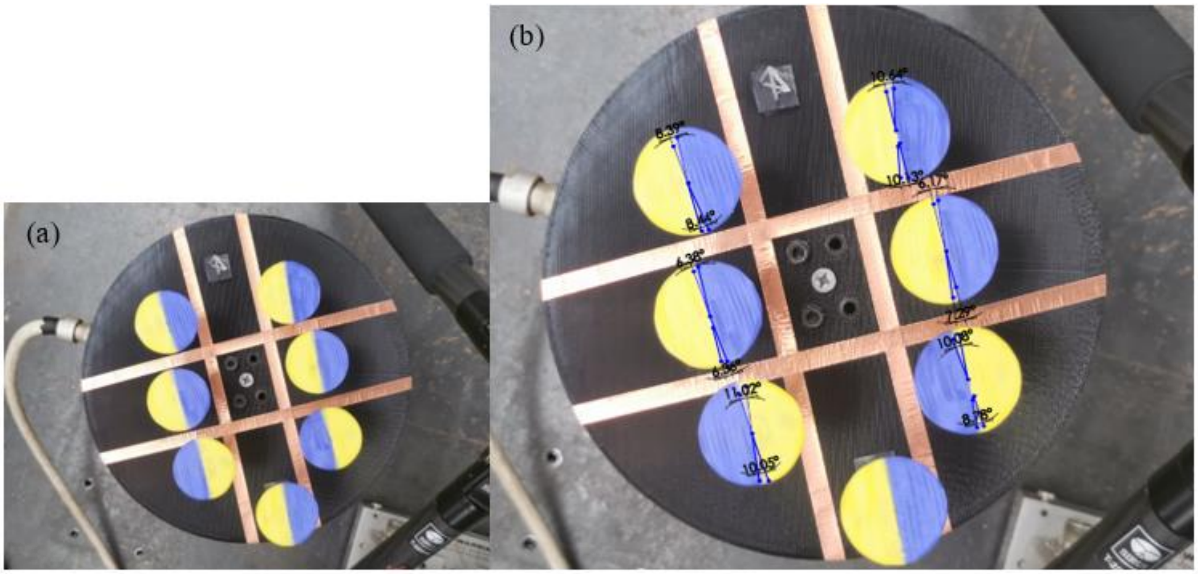

5.2.2 Frequency Measurement Based on Visualized Rotating Angles

As discussed in Section 4.3, the frequency of the excitation can be quantified by the angle formed by the persistence of vision. As shown in Figure 23, each type of rotating column with different top plate thickness shows different rotating angle curves for the same base motion excitation from 0 to 110 Hz. When the frequency of the bottom excitation passes the third resonant frequency of a particular column, its rotation angle changes rapidly as a function. Moreover, for the same frequency change, each structure has a different degree of change in rotation angle. In conclusion, each different excitation frequency corresponds to 5 different rotation angles. Therefore, by measuring the rotation angles of different structures in the experiment and comparing them with the simulated data, the corresponding excitation frequencies can be found. However, this process is based on the fact that the base motion amplitude is already known, as the angle varies with certain excitation amplitude while the frequency is constant. In contrast, in realistic situations, the vibration amplitude of the measured object is usually unknown and even variable during operation, and additional equipment is required to measure the amplitude. Therefore, the rotation angle measured by image processing cannot be directly applied to quantify the excitation vibration frequency unless the vibration amplitude is known. In order to eliminate the process of detecting the vibration amplitude of a target, it is not only necessary to measure the absolute angle of the single structures, but also to calculate the relative angle between different structures. Since all single structures have the same excitation amplitude, the angular ratio between the different types of structures can be used to quantify the frequency. It is possible to select specific structures for harmonic analysis and use frequency sweep simulations at a fixed amplitude to find the rotation angles of different structures at different frequencies, then calculate the ratio of the angles between the structures at different frequencies and finally compare them with the experimental ratio to find the same or approximate values and derive the corresponding frequency, which is the measured frequency. The angle ratio depends on a variety of factors, including the choice of DNA structure used for the measurement, the magnitude of the excitation frequency, and structures that are close to resonance. The detailed principles and measurement process are explained below.

The flow chart for MATLAB code is shown in Figure 24(a). The first step is to enter the average angle of three specific single structures with relatively large angles. The choice of structures is classified into three situations. If the thickness of the top plate for the maximum rotation angle is not the maximum or minimum thickness in the structure, i.e. 1 mm or 5 mm. The structure with the maximum rotation angle will be selected as the specific structure, the remaining two specific structures will then be those where the top plate is one millimeter thicker and one millimeter thinner than the structure. If the thickness of the top plate at the maximum angle of rotation is the maximum or minimum thickness in the structure, then the two other structures with adjacent top plate thicknesses will be used as specific structures in addition to the structure with the maximum angle of rotation. The thickness of the top plate for the structure with the highest rotation angle is also entered.

After entering the values for the three angles, two angle ratios are then calculated, which are respectively entitled X/X+1 and X/X-1, where ‘X’ represents the average angle of rotation for structures with the middle of the three thicknesses, X-1 is the average angle of rotation for structures with a 1mm thinner top plate, and X+1 is the average angle of rotation for structures with a 1mm thicker top plate. Similarly, the simulation results for the corresponding structure with respect to the rotation angle are called up via MATLAB, and the corresponding sets of angle ratios are calculated. The simulated results are derived from Rz values for three specific structures at bottom excitation frequencies of 10 to 110 Hz. The two sets of angle ratios are then used to draw two curves, named simulation curve 1 and simulation curve 2, as shown in Figure 24(b). This plot is designed to help to understand the logic of frequency measurement more clearly. The plot consists of two simulated curves, which come from two simulated arrays, and two horizontal lines from the ratio of the experimentally obtained angles. Simulation curve 1 represents the set of X/X-1 and simulation curve 1 represents the set of X/X+1, where the symbols have the same meaning as the experimental angle ratios. The only difference is that the experimental data are constant values and are represented in the plot by two straight lines, whereas the simulated data are arrays and are represented by two curves.

The measured frequency depends on both the intersections of simulation curve 1 with the experimental angle line x/x-1, and the intersections of simulation curve 2 with the experimental angle line x/x+1. Since curves and lines usually have multiple intersections, it is necessary to eliminate other intersections and determine the final unique intersection, depending on the situation. In the determination process, the first type of intersections have a primary role in measuring the frequency, while the second type of intersections play a secondary role and are mainly used for calibration. For ease of differentiation, the first type of intersections are herein referred to as intersection A, and the second category of intersections as intersection B.

The principles of judgment are classified into the following four scenarios based on the number of intersections. The first case is where the number of intersection points A has only one. In this case, no matter how many intersections B there are, they are not taken into account when estimating frequencies, and the estimated frequency is the frequency of the x-axis corresponding to that unique intersection A. The second situation refers to the fact that there are two intersections of intersection A and only one intersection of intersection B. In this case intersection A with a similar x coordinate to intersection B is chosen. The third case is illustrated in Figure 24(b), where there are two points of intersection A and two points of intersection B. The choice of intersection A in this case is based on choosing the intersection A whose x-coordinates are between the coordinates of the two B points. This basis also applies to the case where there are three intersections A.

When neither of the x-coordinates of the two intersection A is between the intersection B, the average of the x-coordinates of the two intersection B points is calculated, and the intersection A with the x-coordinate closest to the average is selected.

The input and output text of this code are illustrated in Figure 24(c), the input parameters are the thickness of the weight block for the structure with the largest Rz and the three average angles for specific structures. The output includes a value of estimated frequency and the plot such as Figure 24(b). The measured frequencies are accurate to a minimum of one decimal place.

Figure 23

Simulation Results of the Torsion Angle for Five Types of DNA-Shaped Metamaterials

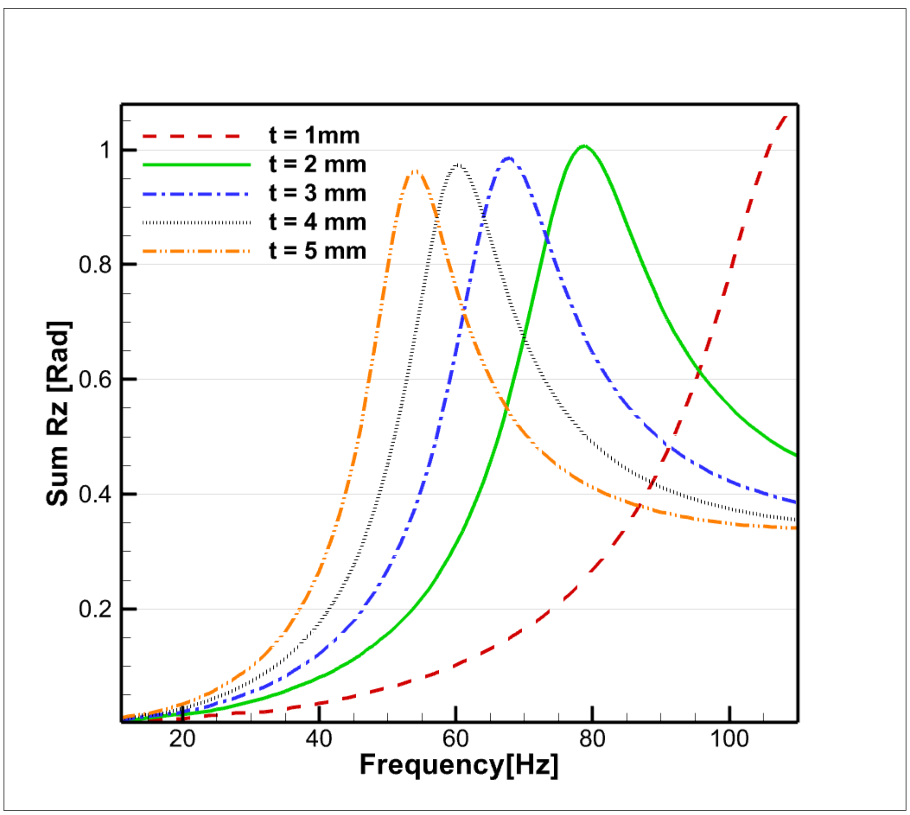

Figure 24

Frequency Estimation Process

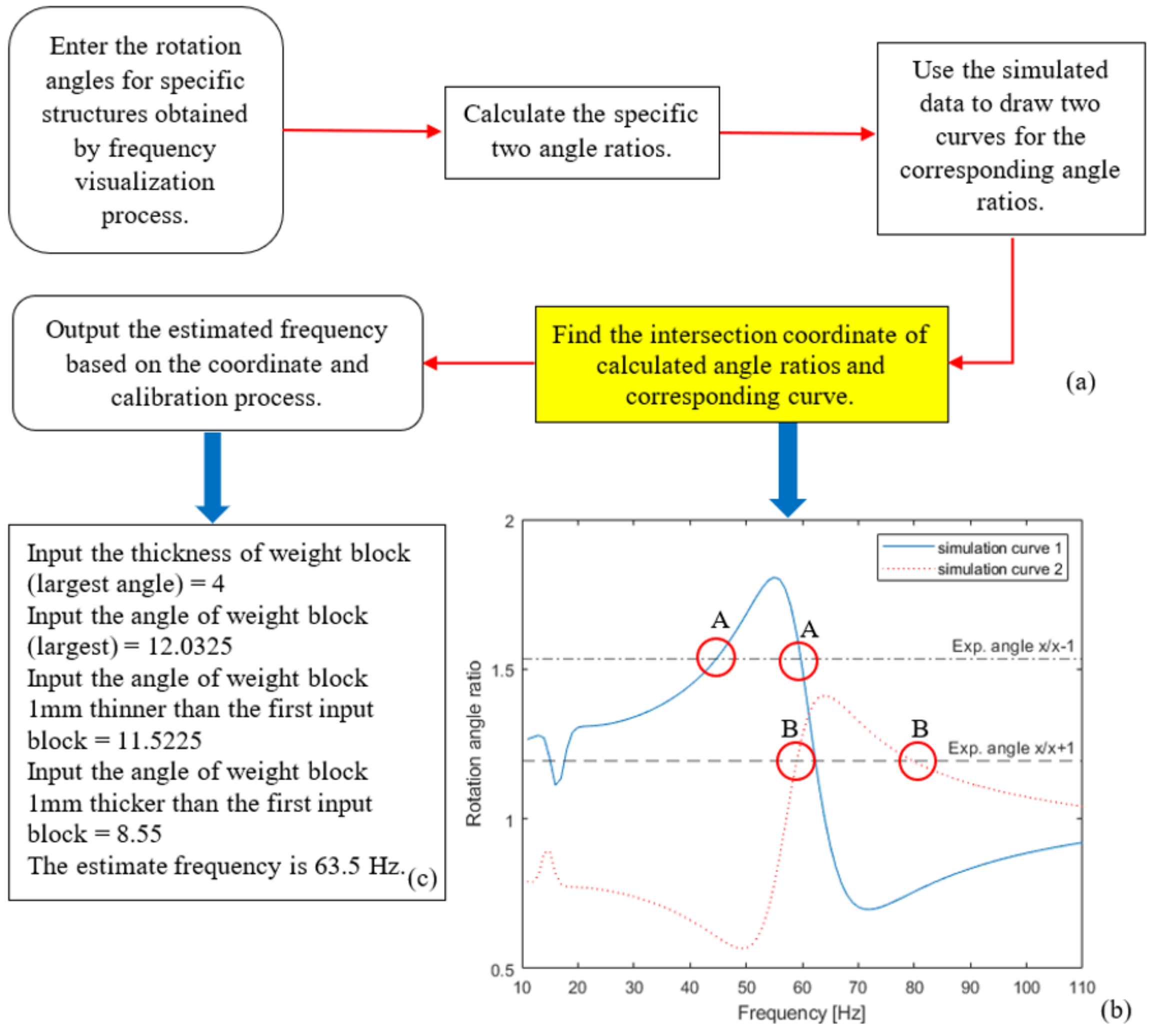

Note. The flow chart for the whole process is shown in figure(a). An illustration of the highlighted step in figure(a) is shown in figure(b). Simulation curve 1 is an array of angle ratios of x/x-1 and simulation curve 2 is an array of angle ratio of x/x+1. ‘x’ represents the rotation angle of the structure with top plate thickness x. Figure(c) shows a sample text of the final output.

Chapter 6

Results and Discussion

6.1 Frequency Visualization Results

According to the comparison of the excitation frequency and the estimated frequency shown in Table 4, it can be found that the minimum error is 0 and the maximum error is 6.32%, and the percentage error varies with frequency as a sinusoidal function as shown in Table 4. It is predicted that the estimated frequencies will have higher accuracy when the bottom excitation frequency is closer to the resonant frequency of a particular structure. This theory is based on the fact that the angle of rotation of the structure changes significantly with frequency when it is close to resonance, while the angle of other structures that are not close to resonance does not change as much. This leads to a large variation in the values of Exp. angle X/X-1 and Exp. angle X/X+1 with frequency, and this theory also applies to the curves formed by the simulation results, so that the difference between the angle ratios corresponding to each frequency at near-resonant frequencies can be large. Therefore, even if the experimental angle ratios have errors due to various factors, e.g., a 10% error from the accurate value, this difference from the real angle ratio will also correspond to a similar frequency when looking for the corresponding simulated angle ratio due to the large variation in the values. The change in measurement frequency accuracy will therefore vary as a sinusoidal function, which follows the same trend as the experimental data. The percentage error in the estimation does not continuously increase or decrease as the frequency changes, but rather peaks and valleys occur as the frequency changes.

Table 4

Excitation Frequency vs. Estimate Frequency, Percentage Error

Excitation frequency [Hz]	Estimate frequency [Hz]	Percentage error [%]
50	52.5	5
55	56.5	3
60	60	0
65	63.5	2.3
70	72.5	3.57
75	75	0
80	77.5	3.125
85	85	0
90	87	3.33
95	89	6.32
100	95.5	4.5

Figure 25

Excitation Frequency, Estimated Frequency and Estimation Error

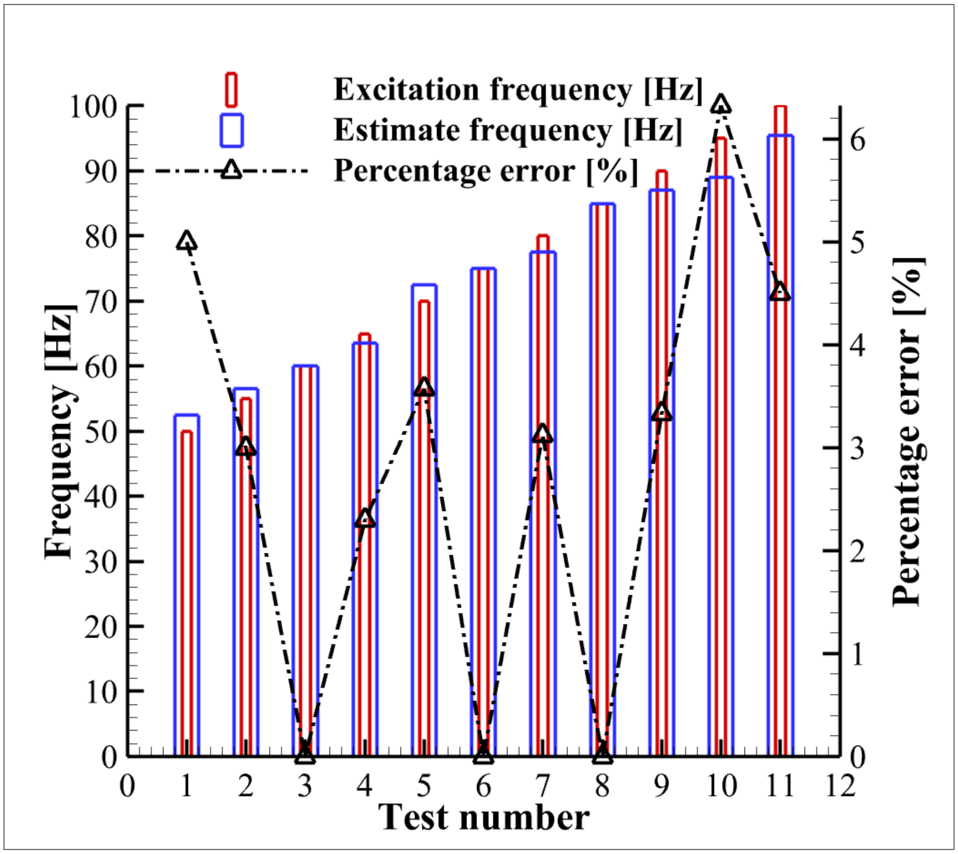

For this experiment, however, the specific frequency values corresponding to the experiments with smaller errors do not exactly correspond to the theoretical resonant frequencies of the structure. Based on the harmonic analysis data, the frequencies for each thickness corresponding to the structure having the maximum rotation angle are: 110 Hz corresponds to 1 mm, 79 Hz corresponds to 2 mm, 68 Hz corresponds to 3 mm, 60 Hz corresponds to 4 mm and 54 Hz corresponds to 5 mm. And the actual valleys correspond to frequencies of 60, 75, and 85 Hz. The explanation for this situation is due to errors in the actual material damping ratio. Firstly, the material damping constant used in the simulation phase is an approximate value derived from the literature and is not an accurate parameter for the material. Secondly, the damping parameters vary as the vibration frequency of the structure changes, whereas the parameters used in the simulations are fixed values. These factors can cause the actual variation in the angle ratio to differ from the simulated situation, resulting in a partial mismatch of values. However, since the frequencies are derived by calibrating several values against each other and the chosen structures are those with relatively large rotation angles, which means that the structures are closer to resonance, these factors keep the errors within manageable limits.

Another factor that creates errors is the quality of the print. Due to the limitations of the printing technology, the actual experiments are subject to errors compared to the simulated situation. These errors due to printing usually include: the printed specifications do not exactly match the simulated structure, the printed gaps between identical DNA structures, as the whole structure cannot be manufactured in one go, but in batches, the material is isotropic in the simulated case but in the real case, as the manufacturing direction is always vertical, when manufacturing the support rods with different orientations, the fabricated structure is not isotropic, the differences in print density between the top plate and the supporting beam due to significant differences in dimensions, whereas in the simulated case this is considered to be the same. These factors can lead to discrepancies between the vibration behavior of the structure in real situations and the simulated situation, resulting in an error between the measured frequency and the actually applied frequency. Similarly, errors in the assembly process can lead to errors in the estimated frequencies, as a single structure cannot be manufactured as a whole. The center of the top plate cannot be guaranteed to overlap with the central axis of the DNA structure, which could cause the top plate not to rotate along the center of the circle and thus lead to errors in the recorded rotation angle and therefore affect the measurement results.

To improve the measurement accuracy of the whole structure, More DNA structures with different top plate weights can be added to the MM array to narrow the gap between the resonance frequencies of different DNA structures. This approach will make it possible to have at least one structure close to resonance at different excitation frequencies. For example, the natural frequencies of structures with 1 mm and 2 mm top plates have a large interval between them, which leads to a maximum measurement error at 85 Hz, by adding a structure with a 1.5 mm top plate thickness, the error is expected to be reduced. Under the limitation of MM array size, the dimensions of individual DNA-shaped structures can be scaled down to place a larger number of MM structures. Moreover, a further experiment could be conducted in the future to measure the actual structural damping ratios at different vibration frequencies to eliminate errors caused by the difference between the actual and simulated damping coefficients. In addition, improvements in printing technology can also reduce measurement errors. More accurate manufacturing can reduce the error in specification between simulated and real structures. Similarly, if the MM array can be printed in its entirety, errors due to the assembly process can be reduced.

6.2 Further Discussion on Frequency Measurement Ranges

After verifying the feasibility of the new vibration measurement technique, an additional simulation process is carried out and the detectable frequency range of a structure with the same DNA structure is investigated. Under the condition that the structural specifications and fabrication materials do not change, the measurable frequency range of the structure is investigated only if the diameter of the support beam and the weight of the top plate are varied. As shown in Figure 26(a), the third natural frequency increases as the diameter of the beam increases. From the CAD model shown in Figure 26(c), it can be seen that the maximum suitable beam diameter is approximately 2.5 mm. Therefore, a modal analysis for structures with beam diameters of 1.5, 2, and 2.5 mm is conducted to find the theoretical measurement range for this type of structure. As it is a simulation, the top plate is treated directly as a mass block and the top plate thickness parameter is converted to the top plate mass. According to the operating principle of the shaker, the amplitude of vibration as shown in Figure 26(b) illustrates the corresponding third mode for structures with three different diameter parameters for top plate masses from 300 to 2750 mg respectively. The minimum weight of the top plate, which determines the maximum third natural frequency of the structure, is set at 300 mg, which is the weight of a top plate with a thickness of 1 mm. The maximum third resonance frequency derived from the simulations is 392.08 Hz and the minimum third resonance frequency is 94.57 Hz. Combined with the previous experiments, it can be concluded that the testable frequencies for this type of structure are approximately 50 to 400 Hz.

Frequency measurements beyond or below the studied frequency are expected to have large errors and the more it is exceeded, the greater the error will be. If the structure is to be used in a higher frequency range, one possible approach is to manufacture the structure by using a resin material with a higher Young's modulus, otherwise, the dimensions of the structure need to be changed to increase the magnitude of d/L. For extremely low frequency working conditions, such as excitation frequency less than 10Hz, the visual persistence phenomenon is not obvious, and the video should be used for rotating angle measurement as an alternative to time-lapse photography.

Figure 26

Simulation Results for Theoretical Detectable Frequency Range

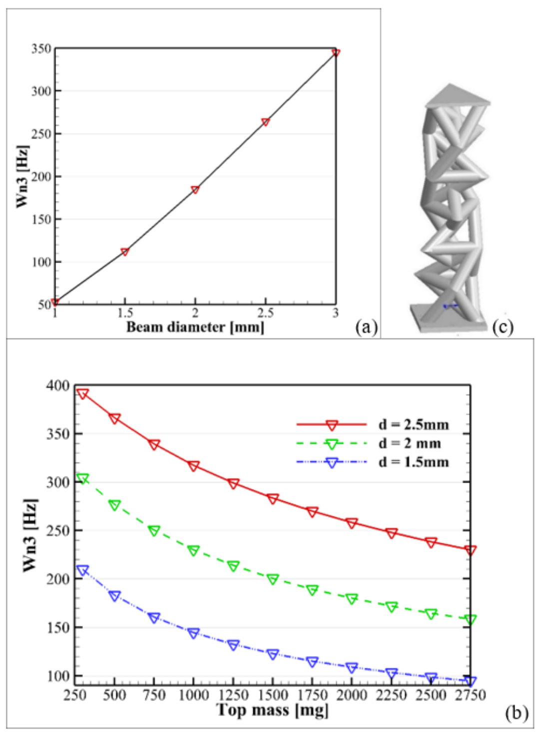

Note. The relation between d and Wn3 is shown in figure (a), the relation between top mass and Wn3 for 3 different d is shown in figure (b) and a sample structure with d=2.5 is shown in figure (c).

Chapter 7

Conclusion

This research develops a new vibration measurement technique involving the design and fabrication of a metamaterial array structure as well as a data acquisition and processing algorithm for frequency estimation. Compared to conventional methods, the advantages of this technique include the rapid detection of the vibration frequency of the target, no need for specialist electronic instruments to capture the vibration signal, highly customizable equipment, and easy operation.

The structure is designed on the basis of simulations and parameter studies and then validated through experiments. Through FEA and 3D printing, a DNA-shaped metamaterial array is designed and fabricated for vibration testing. During the experiment, the structure is fixed to the oscillator, and a vertical bottom excitation is applied to simulate the host-tested structural vibration. The vibration frequency is estimated by the rotation angle of the top plate of the DNA-shaped metamaterials. The experimental results show that the structure has an error of 0-6.32% in measuring frequencies in the 50 to 100Hz interval, which verifies the feasibility of the method. After that, further study is conducted to determine the theoretical frequency detection range by the proposed method but with different structural dimensions. With other structural parameters unchanged, the maximum third natural frequency of the rotating column is determined by varying the mass of the top plate and the diameter of the supporting struts. The simulation results show the possibility of the metamaterial array for detecting vibrations in a wider frequency range, 50-400 Hz.

The current limitations of the new technology can be summarized in the following aspects. First, the quality of the DNA shape structure under vibration is very low because the fabricated material is not specifically designed for the vibration situation. When the excitation vibration frequency is very close to one of its third resonance frequencies, the structure failure will happen. Moreover, the size and performance of the metamaterial array are highly limited due to the low printing quality. In addition, this technique can only be used to measure the vibration frequency in the vertical direction of the target.

Future works include manufacturing process improvement to enhance the print quality of the proposed metamaterial with smaller sizes, research on different materials for vibration testing, research on how to modify the structure to achieve the vibration frequency detection of the target in directions other than the one perpendicular to the attached surface, and the fabrication and tests of samples for different frequency ranges measurement. This developed technology can be expected to be applied in a variety of fields, such as continuous monitoring of the health of building structures, fast inspection of plant machinery, and condition monitoring of vehicles.

Bibliography

Buchan, S. (2013). *Pervasive animation*. New York ; London Routledge Taylor & Francis Group.

Cao, X., Duan, S., Liang, J., Wen, W., & Fang, D. (2018). Mechanical properties of an improved 3D-printed rhombic dodecahedron stainless steel lattice structure of variable cross section. *International Journal of Mechanical Sciences*, *145*, 53–63. https://doi.org/10.1016/j.ijmecsci.2018.07.006

Chen, T., Li, S., & Sun, H. (2012). Metamaterials Application in Sensing. *Sensors*, *12*(3), 2742–2765. https://doi.org/10.3390/s120302742

Cheung, K. W., Starling, M. J., & McGreevy, P. D. (2014). A comparison of uniaxial and triaxial accelerometers for the assessment of physical activity in dogs. *Journal of Veterinary Behavior*, *9*(2), 66–71. https://doi.org/10.1016/j.jveb.2013.11.003

Color Circle Images – Browse 3,929,927 Stock Photos, Vectors, and Video. (n.d.). Adobe Stock.https://stock.adobe.com/ca/search?k=color+circle&search_type=recentsearch&asset_id=23137860

Fan, J., Zhang, L., Wei, S., Zhang, Z., Choi, S.-K., Song, B., & Shi, Y. (2021). A review of additive manufacturing of metamaterials and developing trends. *Materials Today*, *50*, 303–328. https://doi.org/10.1016/j.mattod.2021.04.019

Ferrer, B., Espinosa, J., Roig, A. B., Perez, J., & Mas, D. (2013). Vibration frequency measurement using a local multithreshold technique. *Optics Express*, *21*(22), 26198. https://doi.org/10.1364/oe.21.026198

García, Y. R., Corres, J. M., & Goicoechea, J. (2010). Vibration Detection Using Optical Fiber Sensors. *Journal of Sensors*, *2010*, 1–12. https://doi.org/10.1155/2010/936487

Goyal, D., & Pabla, B. S. (2015a). The Vibration Monitoring Methods and Signal Processing Techniques for Structural Health Monitoring: A Review. *Archives of Computational Methods in Engineering*, *23*(4), 585–594. https://doi.org/10.1007/s11831-015-9145-0

Goyal, D., & Pabla, B. S. (2015b). Condition based maintenance of machine tools—A review. *CIRP Journal of Manufacturing Science and Technology*, *10*, 24–35. https://doi.org/10.1016/j.cirpj.2015.05.004

Hasheminejad, N., Vuye, C., Van den bergh, W., Dirckx, J., & Vanlanduit, S. (2018). A Comparative Study of Laser Doppler Vibrometers for Vibration Measurements on Pavement Materials. *Infrastructures*, *3*(4), 47. https://doi.org/10.3390/infrastructures3040047

Henriquez, P., Alonso, J. B., Ferrer, M. A., & Travieso, C. M. (2014). Review of Automatic Fault Diagnosis Systems Using Audio and Vibration Signals. *IEEE Transactions on Systems, Man, and Cybernetics: Systems*, *44*(5), 642–652. https://doi.org/10.1109/tsmcc.2013.2257752

Hild, F., & Roux, S. (2006). Digital Image Correlation: from Displacement Measurement to Identification of Elastic Properties - a Review. *Strain*, *42*(2), 69–80. https://doi.org/10.1111/j.1475-1305.2006.00258.x

Huang, M., & Yang, J. (2011). Microwave Sensor Using Metamaterials. In *InTech eBooks*. https://doi.org/10.5772/14459

Hunt, C. J., Morabito, F., Grace, C., Zhao, Y., & Woods, B. K. S. (2022). A review of composite lattice structures. *Composite Structures*, *284*, 115120. https://doi.org/10.1016/j.compstruct.2021.115120

Immovilli, F., Bellini, A., Rubini, R., & Tassoni, C. (2010). Diagnosis of Bearing Faults in Induction Machines by Vibration or Current Signals: A Critical Comparison. *IEEE Transactions on Industry Applications*, *46*(4), 1350–1359. https://doi.org/10.1109/tia.2010.2049623

Kumar, S., Lokesha, M., Kumar, K., & Srinivas, K. R. (2018). Vibration based Fault Diagnosis Techniques for Rotating Mechanical Components: Review Paper. *IOP Conference Series: Materials Science and Engineering*, *376*, 012109. https://doi.org/10.1088/1757-899x/376/1/012109

Liu, S., Li, Y., & Li, N. (2018). A novel free-hanging 3D printing method for continuous carbon fiber reinforced thermoplastic lattice truss core structures. *Materials & Design*, *137*, 235–244. https://doi.org/10.1016/j.matdes.2017.10.007

Ma, X., Li, M., Ye, L., Ma, X., Yu, K., Zhu, L., & Song, Y. (2019). Research on Self Calibration Technology for Precision Workpiece Measurement Based on Laser Doppler Vibrometer. *Integrated Ferroelectrics*, *199*(1), 160–171. https://doi.org/10.1080/10584587.2019.1592610

Mohd Ghazali, M. H., & Rahiman, W. (2021). Vibration Analysis for Machine Monitoring and Diagnosis: A Systematic Review. *Shock and Vibration*, *2021*, e9469318. https://doi.org/10.1155/2021/9469318

Saimon, S. M., Ngajikin, N. H., Omar, M. S., Ibrahim, M. H., Mohd Noor, M. Y., Abdullah, A. S., & Salim, M. R. (2019). A low-cost fiber based displacement sensor for industrial applications. *TELKOMNIKA (Telecommunication Computing Electronics and Control)*, *17*(2), 555. https://doi.org/10.12928/telkomnika.v17i2.9754

Saseendran, S., Wysocki, M., & Varna, J. (2017). Cure-state dependent viscoelastic Poisson's ratio of LY5052 epoxy resin. *Advanced Manufacturing: Polymer & Composites Science*, *3*(3), 92–100. https://doi.org/10.1080/20550340.2017.1348002

Slyusar, V. (2009). Metamaterials on antenna solutions. *7th International Conference on Antenna Theory and Techniques*.

Son, K.-S., Jeon, H.-S., Chae, G.-S., Park, J.-S., & Kim, S.-O. (2021). A fast high-resolution vibration measurement method based on vision technology for structures. *Nuclear Engineering and Technology*, *53*(1), 294–303. https://doi.org/10.1016/j.net.2020.06.019

Son, K.-S., Jeon, H.-S., Park, J.-H., & Park, J. W. (2015). Vibration displacement measurement technology for cylindrical structures using camera images. *Nuclear Engineering and Technology*, *47*(4), 488–499. https://doi.org/10.1016/j.net.2015.01.011

Suresh Kumar, N., Naidu, K. C. B., Banerjee, P., Anil Babu, T., & Venkata Shiva Reddy, B. (2021). A Review on Metamaterials for Device Applications. *Crystals*, *11*(5), 518. https://doi.org/10.3390/cryst11050518

Wang, X., Liu, H., & Ouyang, S. (2008). Damping properties of flexible epoxy resin. *Journal of Wuhan University of Technology-Mater. Sci. Ed.*, *23*(3), 411–414. https://doi.org/10.1007/s11595-007-3411-4

Yang, N. (2019). Novel structural design method inspired by DNA and origami. *Results in Engineering*, *4*, 100069. https://doi.org/10.1016/j.rineng.2019.100069

Zhang, P.-L., Li, B., Mi, S.-S., Zhang, Y.-T., & Liu, D.-S. (2012). Bearing Fault Detection Using Multi-Scale Fractal Dimensions Based on Morphological Covers. *Shock and Vibration*, *19*(6), 1373–1383. https://doi.org/10.1155/2012/438789

Appendix A. Detailed Flow Chart

A detailed flow chart illustrates the logic for frequency measurement based on visualization of the rotation angle is shown below.

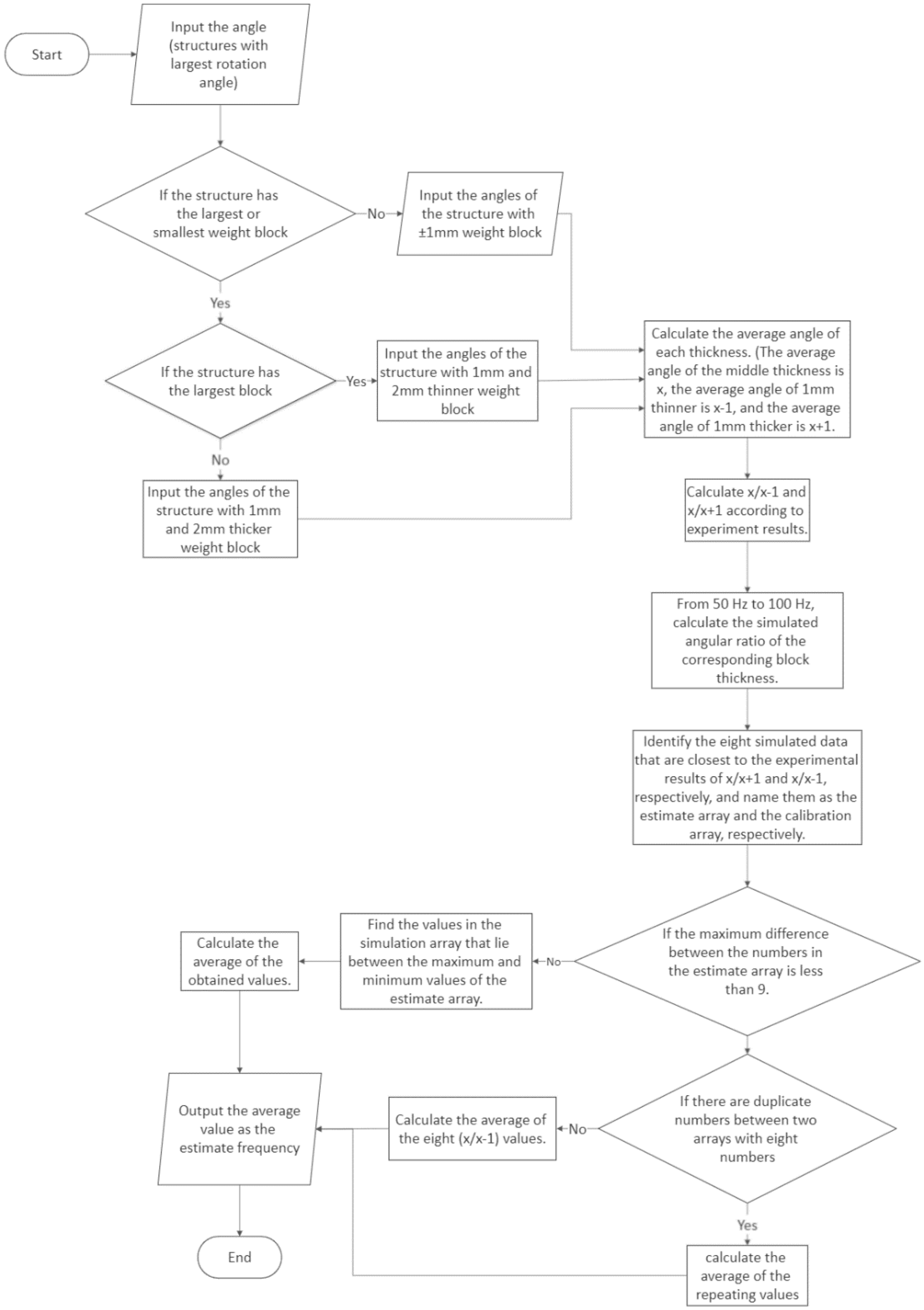
Start
Input the angle (structures with largest rotation angle)
If the structure has the largest or smallest weight block
No
Input the angles of the structure with ±1mm weight block
Yes
If the structure has the largest block
Yes
Input the angles of the structure with 1mm and 2mm thinner weight block
Calculate the average angle of each thickness. (The average angle of the middle thickness is x, the average angle of 1mm thinner is x-1, and the average angle of 1mm thicker is x+1.
No
Input the angles of the structure with 1mm and 2mm thicker weight block
Calculate x/x-1 and x/x+1 according to experiment results.
From 50 Hz to 100 Hz, calculate the simulated angular ratio of the corresponding block thickness.
Identify the eight simulated data that are closest to the experimental results of x/x+1 and x/x-1, respectively, and name them as the estimate array and the calibration array, respectively.
Calculate the average of the obtained values.
Find the values in the simulation array that lie between the maximum and minimum values of the estimate array.
No
If the maximum difference between the numbers in the estimate array is less than 9.
Output the average value as the estimate frequency
Calculate the average of the eight (x/x-1) values.
No
If there are duplicate numbers between two arrays with eight numbers
Yes
End
calculate the average of the repeating values